Laboratory Study of Laser-Scattered Light by Rough Surfaces

Kamei, Akihide

博士論文

Laboratory Study of Laser-Scattered Light by Rough Surfaces

平成１２年１月

神戸大学大学院自然科学研究科

亀井　秋秀

Akihide Kamei

博士論文

Laboratory Study of Laser-Scattered Light by Rough Surfaces

（レーザー光による不規則物体の散乱過程）

Akihide Kamei

The Graduate School of Science and Technology,
Kobe University, Nada, Kobe, 657-8501 Japan

Contents

1 General Introduction

This thesis is dedicated to understand the light scattering by surfaces of small bodies in the solar system. It is known that most atmosphereless bodies in the solar system are covered with regolith layers generated by impacts of meteors. The study of light scattering by such regolith surfaces, therefore, is an important subject to investigate surface materials and surface structure of such bodies. The light scattered by these surfaces can be described by the equation of radiative transfer (Chandrasekhar 1960), but the solution of this equation requires that the particle single-scattering albedos and phase functions be specified.

Light scattering by single particles is well understood for perfect spheres of any size. For most such particles Mie theory provides a first-order description (Pollack and Cuzzi 1980) that is adequate for most radiative transfer calculations. It is the exact, mathematical solution of Maxell's equations for the case of the interaction of a plane electromagnetic wave with a uniform spherical particle of arbitrary size and refractive index. This solution is derived and discussed in many text (Van de Hulst 1957, Bohren and Huffmann 1983). The inputs to the solution are the size parameter, $X = \pi D/\lambda$, and the complex refractive index $m = n + ik$, where D is the particle diameter, λ is the wavelength, and n and k are the real and imaginary parts of the refractive index, respectively. A powerful technique for calculating the scattering properties of an irregular shaped particle comparable to the wavelength in size is the discrete dipole approximation (Purcell and Pennypacker 1973, Draine and Goodman 1993), in which the particle is synthesized by an array of dipoles.

The main focus of this study is to examine the light scattering by planetary regoliths. However, it is not established how the scattering properties of an isolated particle are related to the average properties of an ensemble of similar particles in a close-packed powder or regolith. This question has never been satisfactory answered, although the available evidence suggests that they are similar. It is found that the intensity and the state of polarization of light scattered from a solid surface depend on the scattering geometry, the optical constants of surface materials, and the surface texture. There have been several laboratory studies for lunar, meteorite, and terrestrial samples (Dollfus *et al.* 1989, Egan *et al.* 1973, French 1980, Geake and Dollfus 1986, Verbiscer and Veverka 1990). Theoretical treatments of bidirectional reflectance have been summarized by Hapke (1993). His model provides an approximate method for light scattering deduced from the radiative transfer theory. Its method is most widely used in the analysis of planetary photo-polarimetry to study the scattering of light from rough, particulate surfaces and to investigate the relating photometric behavior to physical and geological properties of the surface terrains.

In recent years, the detailed features of the surface of small bodies in the solar system appeared from disk-resolved data by spacecraft observations (Clark *et al.* 1999, Helfenstein *et al.* 1994, 1996, Simonelli *et al.* 1998). The Japanese mission for asteroid sample return (MUSES-C) will be launched in 2002. The primary goal of the MUSES-C is to acquire and verify the technologies, which are necessary to collect the samples from a

small body in the solar system and bring them back to the Earth. The mission target is the asteroid (10302) 1989ML. This is a small near-Earth object with diameter of 1 km or less, and, it is believed, this asteroid keeps the record of the state of the early solar system. MUSES-C will carry a CCD camera, Asteroid Multiband Imaging CAmera (AMICA), to obtain the images of the target asteroid. Visible-near infrared ($0.36 - 1.02$ μm) photo-polarimetry will be performed by using this camera. Furthermore the observation by using LIDAR (LIght Detection And Ranging) is also planned. The LIDAR instrument has an intrinsic purpose to measure a distance from the spacecraft to the asteroid. In addition, it has a capability to detect the surface roughness and its albedo at a wavelength of 1 μm. The *in situ* photometric and polarimetric measurements of the surface of the target asteroid are available both for characterizing the asteroid itself and deciding the sampling sites. Therefore, laboratory study of light scattering by various types of rough surface analogue for asteroid surfaces is strongly required to supply the data for simulation of surface physical properties.

In order to study the basic scattering properties of rough surfaces and provide reference data for the *in situ* photo-polarimetry planned by MUSES-C mission, I have performed laboratory measurements of light scattering by rough surfaces by using a goniometric photopolarimeter. The sample rough surface is illuminated by a He-Ne laser beam at a wavelength of 632.8 nm and the resulting scattered light is detected by a photomultiplier. A plane defined by the light source - the sample - the detector is called the scattering plane. The zenith angle of both the light source and the detector can be changed their positions from 0° to 90°, independently. I use as samples the several different kinds of rough surfaces, *i.e.* plates with different degrees of surface roughness, particulate layers consisting of irregular shaped particles with different radii, and the particulate layers on the rough plates.

I have also analyzed the light scattering by rough surfaces by comparing my results of laboratory measurements based on Hapke's bidirectional reflectance model with theoretical values and observational data. Referring to the resulting values of Hapke parameters for particulate surface of interest deduced from the comparison of laboratory data with those derived from the theoretical analysis, I have examined the applicability of Hapke's model and interpreted Hapke parameters deduced from the observational data.

In section 2, the instruments used for laboratory measurements are explained in detail. The reliability of the data obtained by this instrument is discussed.

In section 3, it is reported the results of the measurements of scattered light reflectance for different types of surfaces consisting of the plates and the particles made of alumina (Al_2O_3). The measurements were done by varying the incident angle at a fixed phase angle, and also changing the phase angle at a normal incidence. In order to simulate the surface structure of small asteroids covered with a thin regolith layer, two-component surface models, *i.e.* plates covered with thin layer of the particles, were made and examined.

In section 4, I demonstrate how the value of retrieved Hapke parameters depends on the

3

range of phase angle in the measurements. Bidirectional reflectance of surfaces consisting of olivine, graphite, Allende meteorite, and Gao meteorite powder were measured in the wide $(2° - 155°)$ and narrow $(2° - 80°)$ range of phase angles.

In section 5, referring to our laboratory measurements of layers consisting of olivine and graphite particles with different size distributions, I investigate several kinds of empirical relations between the parameters in the polarization-phase curve and the surface albedo, with emphasis on clarifying the effect of particle size on the surface. The aim of this work is to find suitable conditions of the observation and the best choice of polarization-phase curve parameter for estimating the surface properties of the target asteroid from the planned polarimetric observations by MUSES-C, which are limited in the coverage of phase angle and the total number of the observations.

2 Experimental Procedures

2.1 Instruments

The experimental setup used for measurements in this paper is illustrated in Fig. 2.1. The apparatus consists of a goniometric photopolarimeter (Nakamura *et al.* 1999). Two aluminum arms attached to two goniometers, respectively. One arm supports the light source and the other one supports the detector. Each of arms can be moved from $\pm 90°$ from the zenith position. A sample holder is placed between the goniometers. The holder can be tilted $\pm 25°$ from the horizontal position in the parallel or perpendicular direction to the arms. Within the above tilt angle, most particulate samples are expected to be stable, because the typical angle of repose is $25° - 30°$ (*e.g.* Statham 1974). The center of the rotation of the arms is situated on the average sample surface in a tray above the sample holder. The light source, the sample, and the detector define the scattering plane and the angles of interest are the zenith angle of incident ray i, the zenith angle of emergent ray e, and the phase angle g, *i.e.* the angle between the light source and the detector. The minimum phase angle achieved for the central point of the sample is $1°$ for the moment, and will be made smaller by future rearrangement of the system.

The light source is a 4 mW He-Ne laser at a wavelength of 632.8 nm with three possible beam diameters. The beam diameter of the laser is typically about 2 mm. The collimated beam of about 1 cm diameter is available by attaching a beam expander to the laser. The laser is fixed directly to the arm. In the widest beam mode, the light from the laser is expanded and collimated by optics on the arm. The beam diameter is typically about 6 cm.
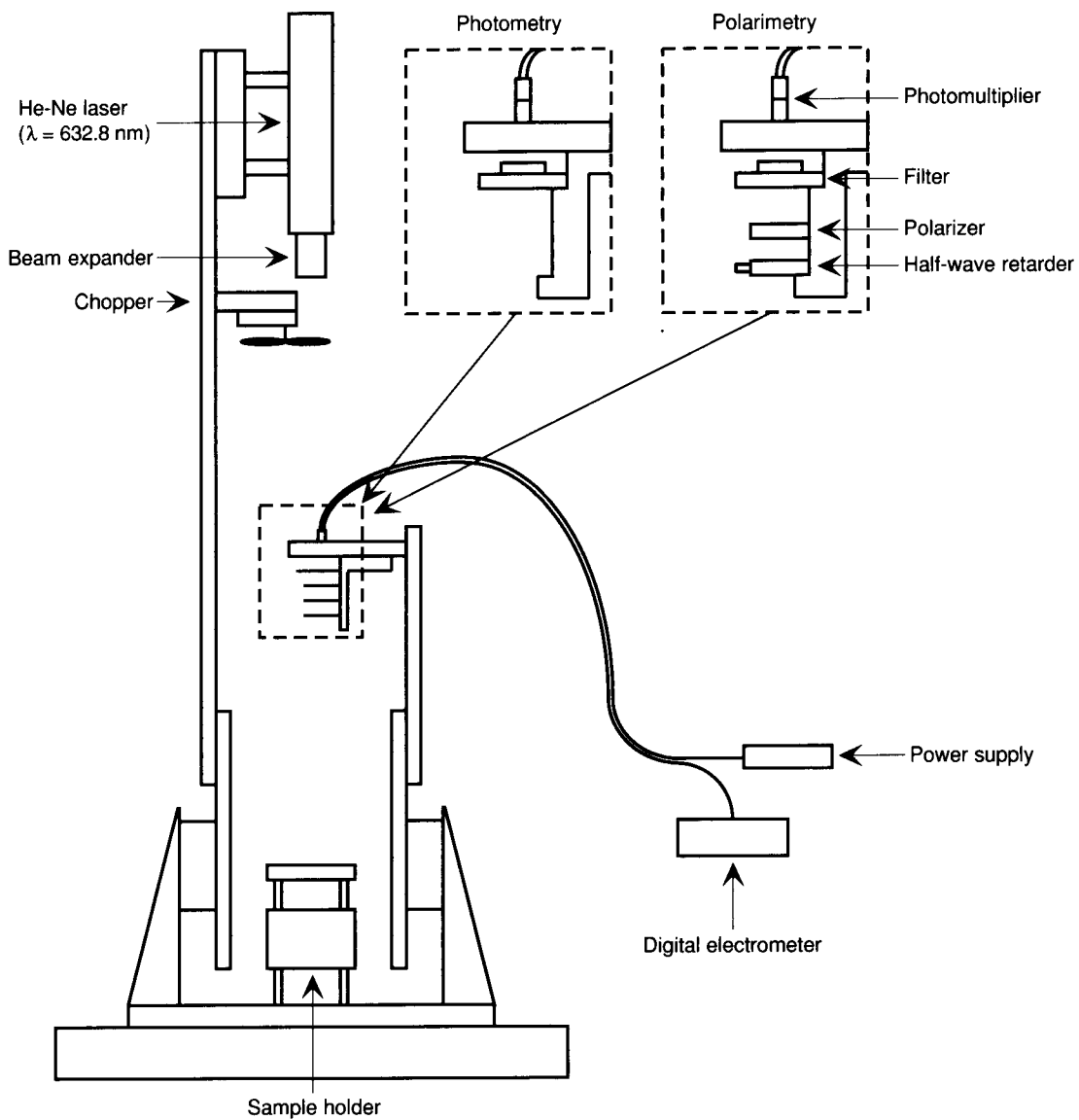
The detector is a photomultiplier with a sensitive surface of 8 mm in diameter. Placing a narrow band filter of 1 nm FWHM in front of the detector minimizes the background light. An aperture in front of the narrow band filter adjusts the field of view (FOV) of the detector. A half-wave retarder and a polarizer are inserted between the sample and the detector optionally for the polarimetric measurement. The optical signal of the detector is digitized by a digital electrometer. We have a chopping mode in which the incident beam is chopped by a fan, to measure the optical signal and the dark level (dark current and background light) by turns with a cycle of 1/30 Hz (Fig. 2.2).

The reflectance is calibrated using a standard white surface made of Ba_2SO_4. The reflectance of its surface is known to be having 100.0% of Lambert albedo at the condition for incident and emergent angle of $0°$ and $45°$, respectively.
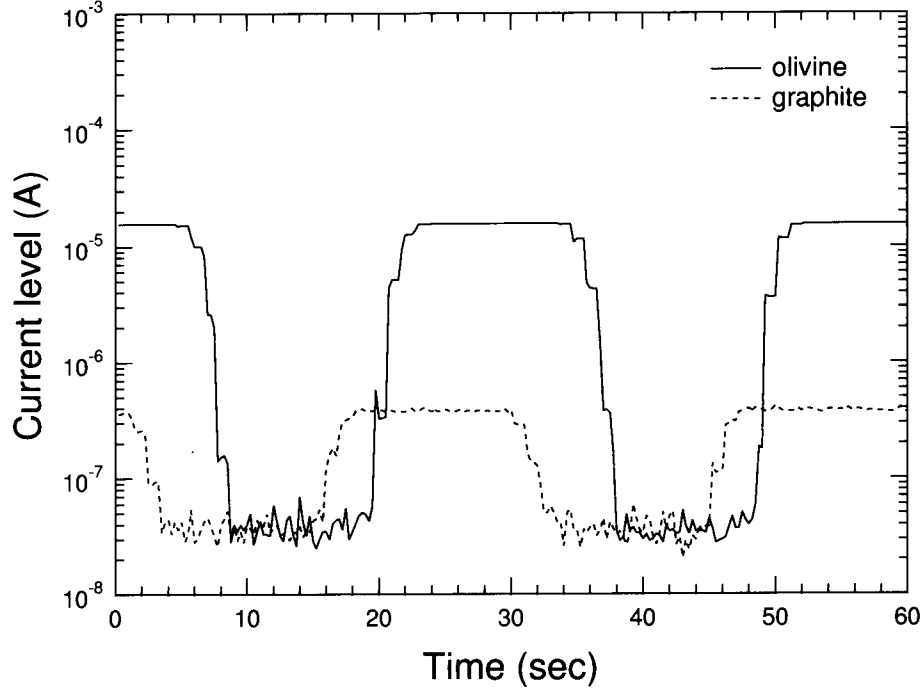
2.2 Performance

We checked the dark level, the stability, the sensitivity, and the linearity of the experimental setup as follows. The light source power after the beam expander was measured by a digital spectrometer and was 0.5 mW. The power of the incident laser beam was changed more than 3 orders of magnitude using three neutral density (ND) filters with transmissivity of 1, 10, and 30%, respectively, and their combinations (the total transmissivities were then between 0.03 and 100%). To obtain the dark level, we put a mask between the light source and the surface. For each of the configurations, the output cur-

He-Ne laser
($\lambda = 632.8$ nm)

Beam expander

Chopper

Photometry

Polarimetry

Photomultiplier

Filter

Polarizer

Half-wave retarder

Power supply

Digital electrometer

Sample holder

Fig. 2.1. Schematic view of experimental setup.

Fig. 2.2. Raw data of measurements of olivine and graphite particulate layers, showing the optical signal and the dark level.

rent of the photomultiplier was sampled 500 times with 4 Hz rate. Within one sampling sequence, which took a minute, the fluctuation of the dark level was less than 1% (Fig. 2.3). The fluctuation of the signal, $i.e.$ the laser power multiplied by the detector sensitivity was 0.01%. The fluctuation of the signal for a 100-minute-run was 1.4% (1σ) (Fig. 2.3). The expected intensity of the reflected light at the detector position was calculated and compared with the output current of the photomultiplier. Thus obtained sensitivity was $\sim 10^3$ A/W at applied voltage of 1300 V, which is within the same order of magnitude with the value in the catalogue. The linearity was within 1% in the above measurements with ND filters (Fig. 2.4). We measured the reflected light of the alumina (Al_2O_3) plate covered by black papers with different diameter of circle to check the field of view (FOV) of the detector (Fig. 2.5).

This experimental setup is enable to measure the intensity and the state of polarization of the scattered light. Since the solid angle seen by the detector is larger than the spot size of the incident light, it is necessary to correct the observation geometry to obtain the reflectance $r(i, e, g)$ from the optical signal of a sample $I(i, e, g)$ as follows.

$$
\begin{aligned}
r(i, e, g) &= r_{Lambert}(0°, 45°, 45°) \, \frac{\cos 45°}{I_{Lambert}(0°, 45°, 45°)} \, \frac{I(i, e, g) \, \cos i}{\cos e} \\
&= \frac{1}{\pi} \frac{\cos 45°}{I_{Lambert}(0°, 45°, 45°)} \, \frac{I(i, e, g) \, \cos i}{\cos e}
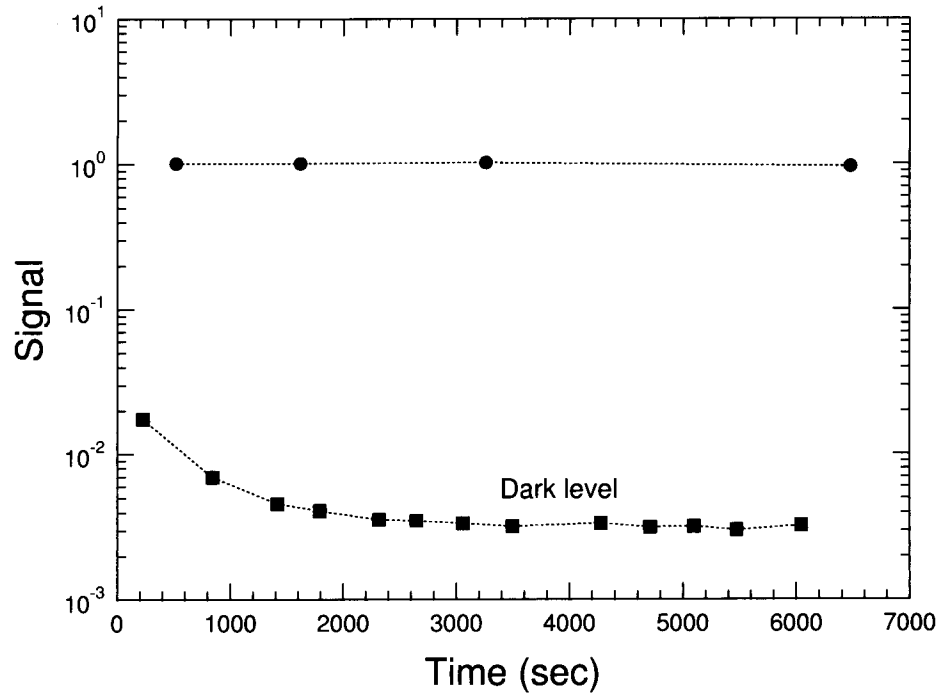\end{aligned}
$$

7

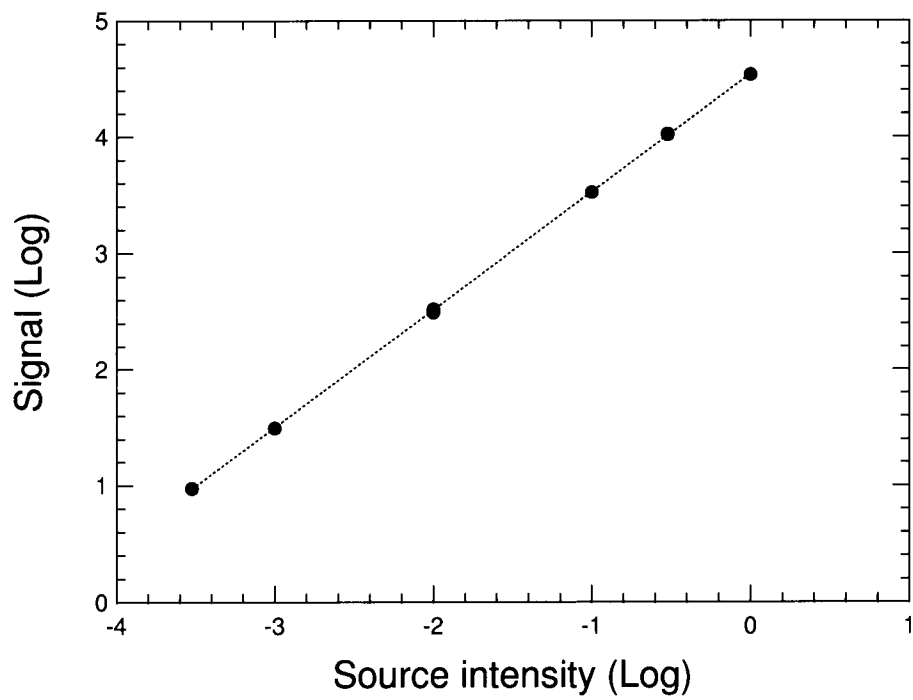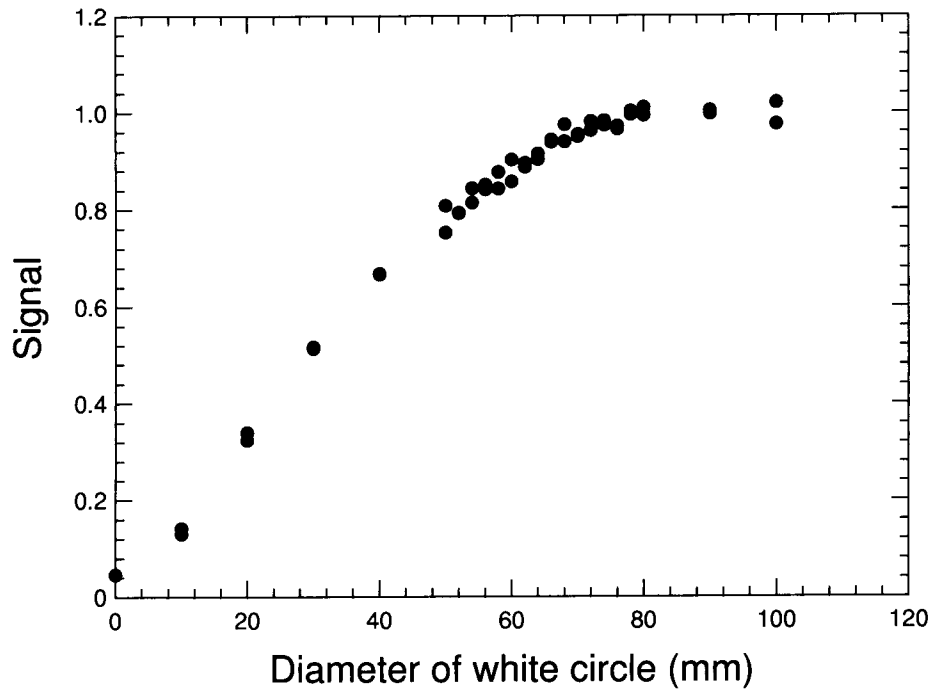**Fig. 2.3.** Stability of the light source and the dark level.

Fig. 2.4. Linearity of the light source.

Fig. 2.5. Field of views (FOV) of the detector was designed to be 80 mm in diameter. The laser beam was expanded approximately to 60 mm in diameter. The detector signal increases with the diameter of the white circle until it reaches 80 mm.

3 Photometric Measurements of Rough Surfaces Made of Alumina Plates and Particles

3.1 Introduction

Most atmosphereless bodies in the solar system are covered with regolith layers. Light scattering by regolith layers is an important subject to investigate surface materials, structure, and size of regolith of such atmosphereless bodies. Especially at very small phase angles, a nonlinear increase in the intensity of light scattered from a particulate medium, the opposition effect, occurs as the phase angle decreases to $0°$. Most solar system objects whose surfaces can be seen and whose photometric functions have been measured at small phase angles exhibit this phenomenon. Laboratory studies for most terrestrial materials show an increase of reflected intensity at small phase angles (Oetking 1966, Dollfus et al. 1989). Theoretical treatments have been summarized by Hapke (1993). It has been suggested that both shadow hiding and coherent backscattering are viable mechanisms for producing an opposition effect (Hapke et al. 1998).

The Japanese mission for asteroid sample return (MUSES-C) will carry a CCD camera to return images of the target asteroid (Fujiwara et al. 1998). Visible photo-polarimetry will be performed by this camera. The nominal and backup mission targets are Nereus and 1989ML, respectively. Both are small near-earth objects with diameter of 1 km or less. It is possible that on such a small object with little surface gravity, the process of the regolith development is different from that on other objects such as the Moon. Therefore, detailed study of light scattering by various types of regolith layers, especially for a thin layer of regolith, is required. In order to study the scattering properties of rough surfaces covered by small grains, and their dependence on the incident angle of the light source, phase angle, roughness, and presence of regolith layer, we have done laboratory measurements of light scattering by rough surfaces. It is expected that we can get information about the surface conditions such as the size distribution, the porosity, and the thickness of regolith layer by taking images in a condition of small phase angle at which the opposition effect occurs. Here we present a report of our photometric measurements at small phase angle by varying the incident angle and at normal incidence by varying the phase angle to verify this expectation.
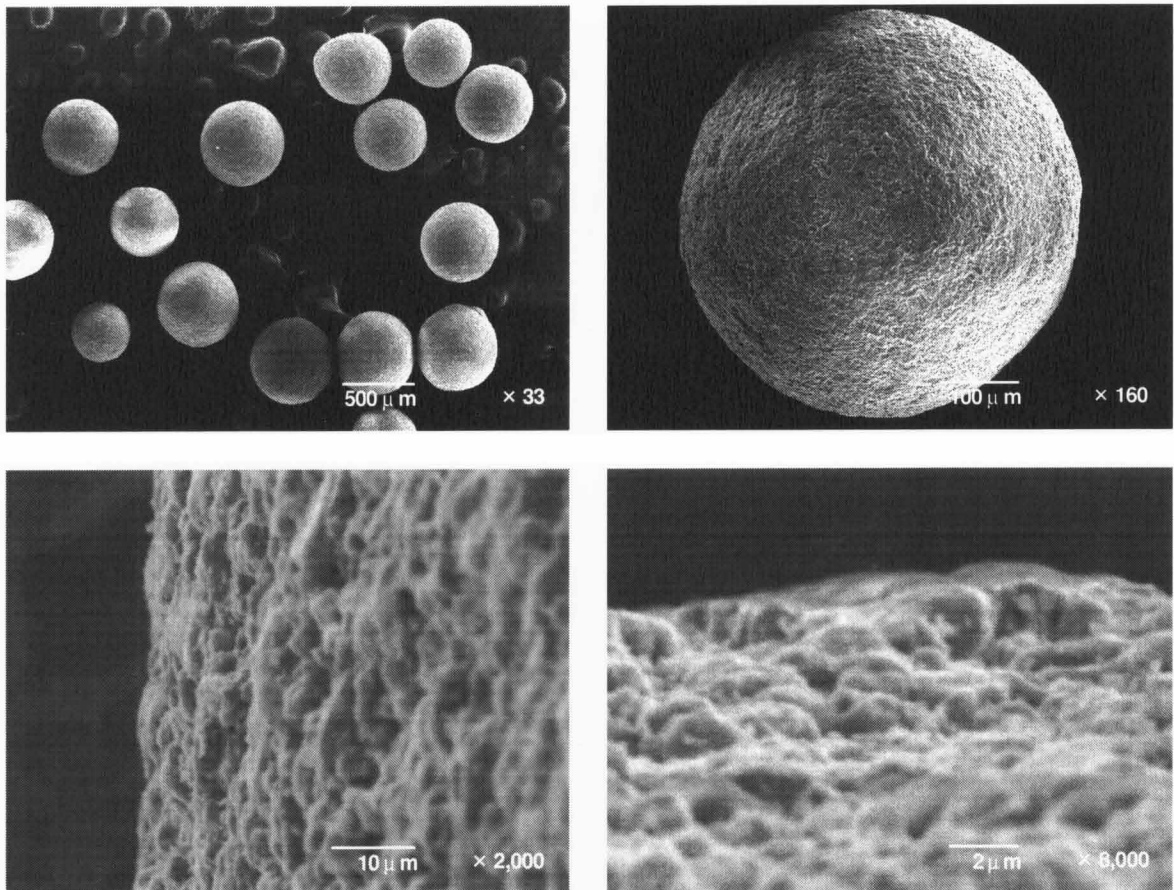
3.2 Measurements

The instruments used for our laboratory measurements are described in the previous section (see section 2). In this work, the beam expander was placed in front of the light source. The laser beam was expanded to a typical spot diameter of 1.6 cm on the sample, which is sufficiently large, as compared with the size of the individual particles on the rough surface, while the detector viewed a much larger area.

The samples prepared for the measurements are different types of scattering surfaces made of alumina (Al_2O_3) summarized in Table 3.1. Scanning electron micrographs of particles with mean diameters of 500 μm are shown in Fig. 3.1. The optical constants of alumina read from the table and the figure from Gervais (1991) are $n = 1.766$ and k being unknown accurately but estimated to be smaller than 0.01 at 633 nm. The surface

Table 3.1 Samples used for measurements.

Samples			
Material	**Refractive index**	**Type**	**Surface roughness, R_a**
alumina (Al_2O_3)	$n = 1.766$ $k < 0.01$	plate	0.075 μm
			0.335 μm
			1.965 μm
		Type	**Diameter** / **Porosity**
		particle	500 μm (average) / 0.44
			45 μm (average) / 0.80
			0.1 μm (maximum) / 0.98

Fig. 3.1. Electron photomicrograph of alumina particles with mean diameters of 500 μm.

11
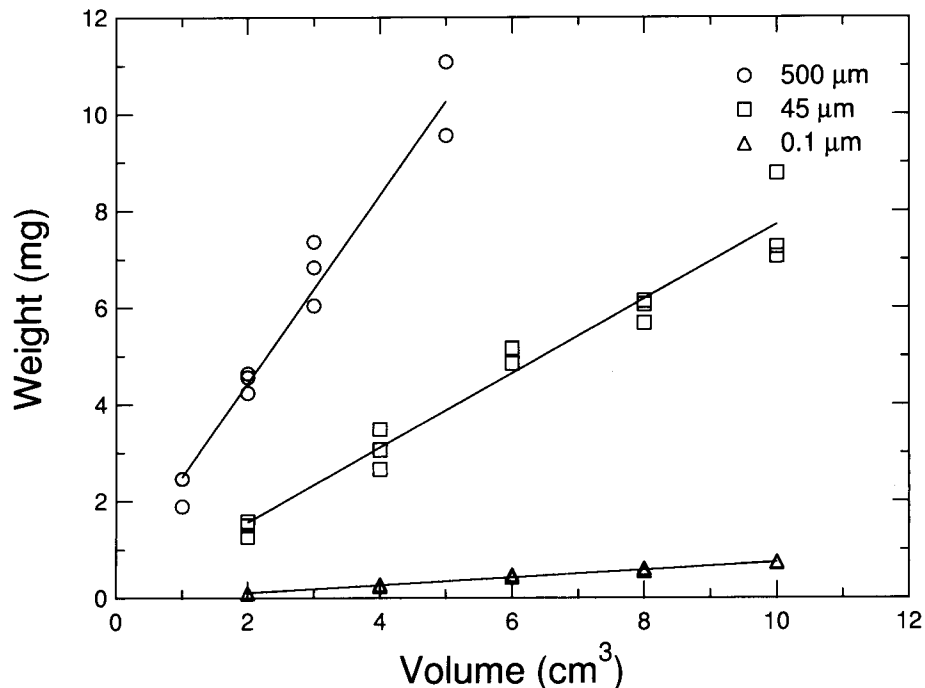
Fig. 3.2. Weight measurements of alumina particles.

roughness is defined by the arithmetic mean roughness R_a, *i.e.*

$$R_a = \frac{1}{l} \int_0^l |f(x)| \, dx$$

where $f(x)$ is the function of surface roughness (a height distribution of the surface measured from a reference horizontal level along a line X) and l is the length of the surface along the line X for which the measurement is performed. We estimated the porosity of alumina particles by measuring the weight versus volume and using the specific gravity of alumina, 3.9 g/cm^3 (Fig. 3.2). Here the porosity p is given by $p = 1 - w/3.9v$, in which w is the weight and v is the volume. Also we prepared six two-component surface models in order to simulate the structure of small asteroids covered with a thin regolith layer, that is, two different composite surfaces; one with mean diameters of 45 μm and the other with maximum diameters of 0.1 μm particles. We measured the total volume of the particles to control the thickness of the particle layer. The average thickness was about 100 μm for both size of particles.

3.3 Incident angle dependence of backscattered light

Firstly we investigated the behavior of backscattered light at small phase angle by regolith layers as a function of incident angle. The phase angle was fixed at 1°, and the photometric measurements were performed by varying incident angles to the surface ranging from 0° to 70° by using rotating arm stages. The solid angle seen by the detector was 0.4° which was smaller than the phase angle.

Figures 3.3 – 3.6 show the results of the backscattered light reflectance dependence on incident angle for twelve conditions of surface. Measurement errors are less than the size of the symbols. In case of plates with different roughness (Fig. 3.3), while depending on the roughness, the reflected light shows an increase observed at $i = 0°$, probably due to Fresnel specular reflection, and decreases as the incident angle increases. The Fresnel specular reflection, which should be occurred when the incident angle is equal to the emergent angle, can be explained by origination from the roughness of the plates or the inclination of the surface normal from the zenith. The specular amplitude is particularly strongest in case of the smoothest plate and weaker as the plate is rougher. In case of particulate layers with arbitrary thickness (Fig. 3.4), the reflectance decreases as the incident angle increases, but rather approaches a Lambert reflectance as compared with that of the plates. The absolute reflectance of the 45 μm particle layer is stronger than the 500 μm particle layer and also stronger than the 0.1 μm particle layer. The causes are not solved yet but the former may be due to the effect of the single-scattering albedo which is larger as the size parameter is smaller or the phase function of the particles which also changes its shape with the size parameter. The latter cannot be explained by the size parameter, and may be due to the difference of porosity between the samples. Figures 3.5 and 3.6 show the backscattered light reflectance for 45 μm particle layer and 0.1 μm particle layer on three plates with different roughness. The specular amplitude appears to be more effectively reduced by 45 μm particles than by 0.1 μm particles. It may be due to the effect of the porosity or the phase function. The reflected light of each case has an effect of Fresnel specular reflection by the plate at small incident angle, and decreases as the incident angle increases but the rate of decrease is smaller than that of the bare plate.

3.4 Phase angle dependence of scattered light

Secondly we investigated the phase angle dependence of scattered light by regolith layers. The incident angle was fixed at 0°, and the photometric measurements were performed by varying emergent angles to the surface, that is the phase angles, ranging from 1° to 70°.

Figures 3.7 – 3.10 show the results of the scattered light reflectance dependence on phase angle for twelve conditions of surface. In these results, measurement errors are also less than the size of the symbols. In case of plates with different roughness (Fig. 3.7), the reflected light increase at very small phase angles, probably affected by Fresnel specular reflection. The specular amplitude of the smoothest plate is particularly strongest and weaker as the plate is rougher. In case of particulate layers with arbitrary thickness (Fig. 3.8), the reflectance of 45 μm particulate layer increases as the phase angle decreases. It is caused by opposition effect due to interparticle shadow hiding. The reflectance of 500 μm and 0.1 μm particulate layers, however, almost never show the opposition effect. Figures 3.9 and 3.10 show the scattered light reflectance for 45 μm particle layer and 0.1 μm particle layer on three plates with different roughness, respectively. The effect of Fresnel specular reflection at very small phase angles is diluted by the existence of a particulate layer, but the opposition effect by 45 μm particulate layer is added as the phase angle decreases.
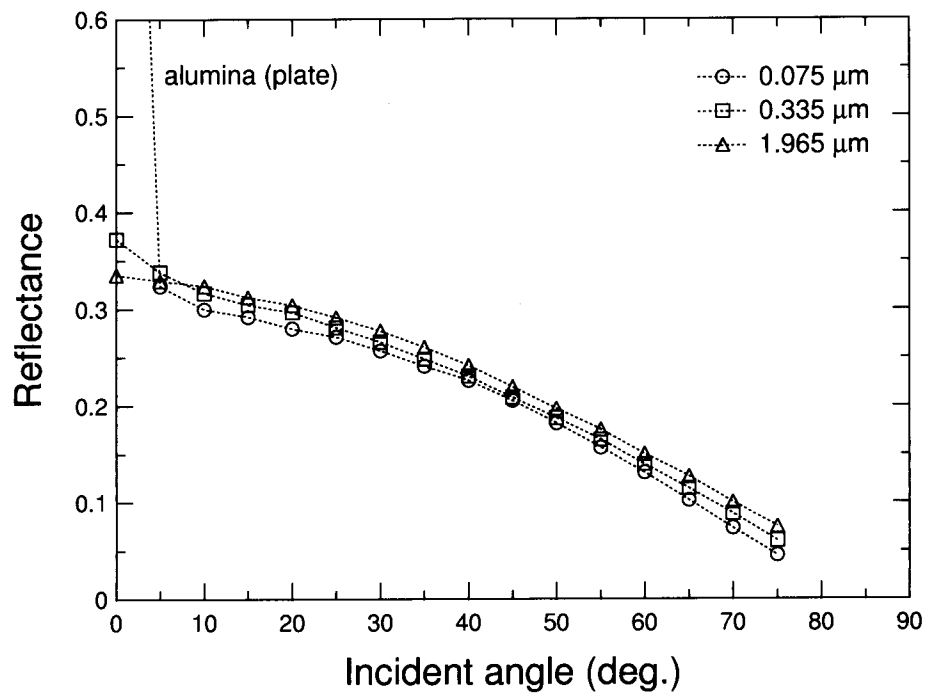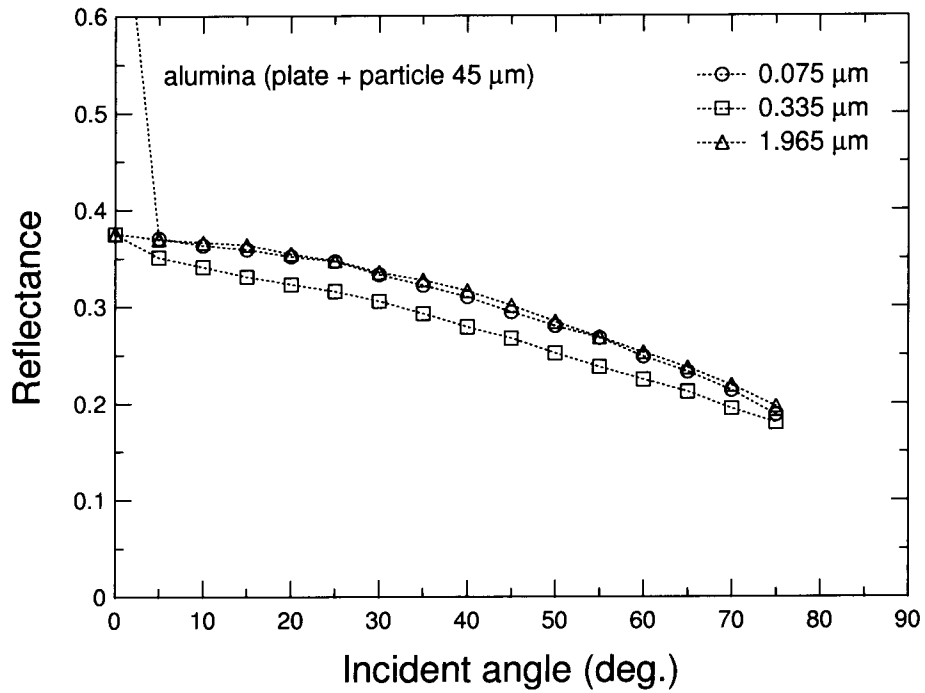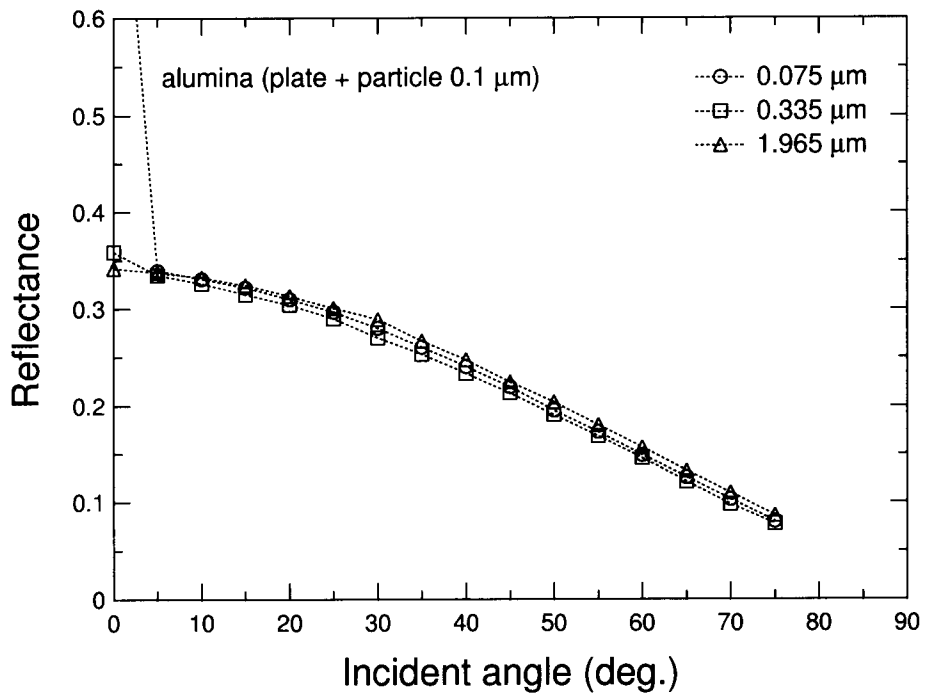
Fig. 3.3. Backscattering reflectance as a function of incident angle for alumina plates with different surface roughness.
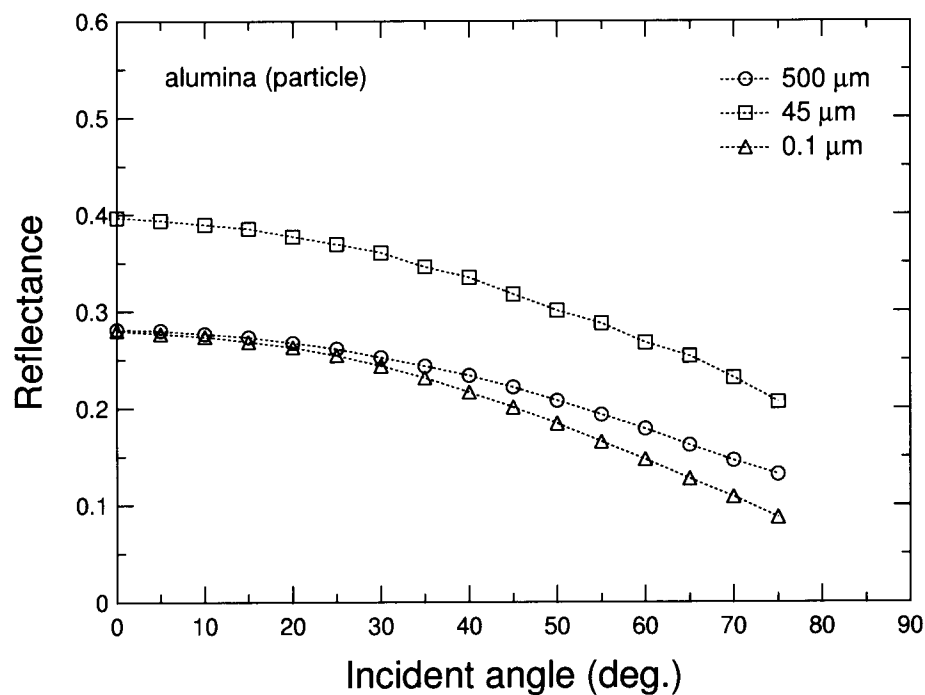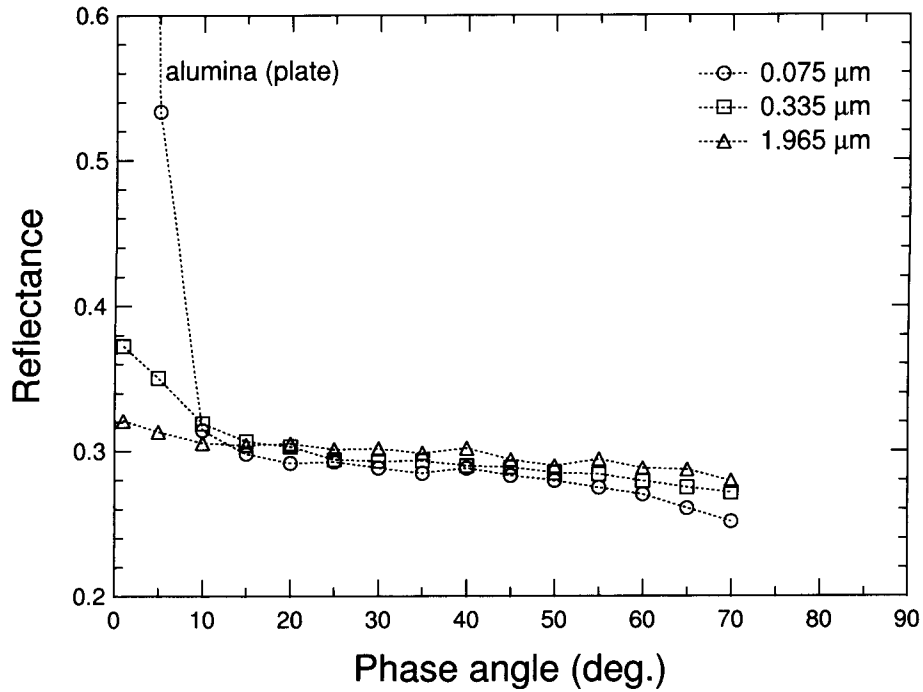

Fig. 3.4. Backscattering reflectance as a function of incident angle for alumina particles with different diameter.
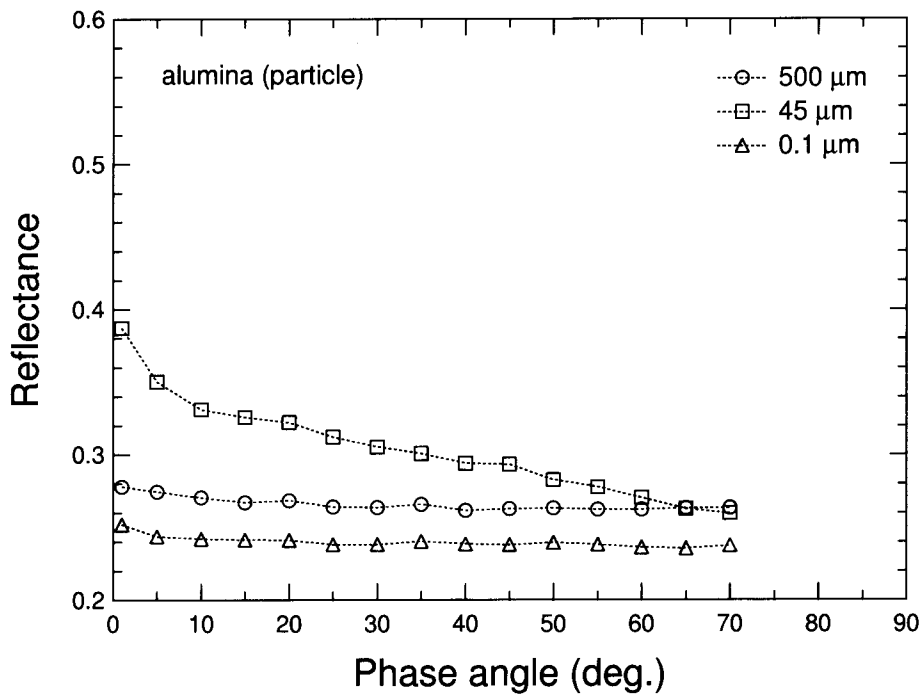
14

Fig. 3.5. Backscattering reflectance as a function of incident angle for alumina particle with diameter of 45 μm on plates with different surface roughness.
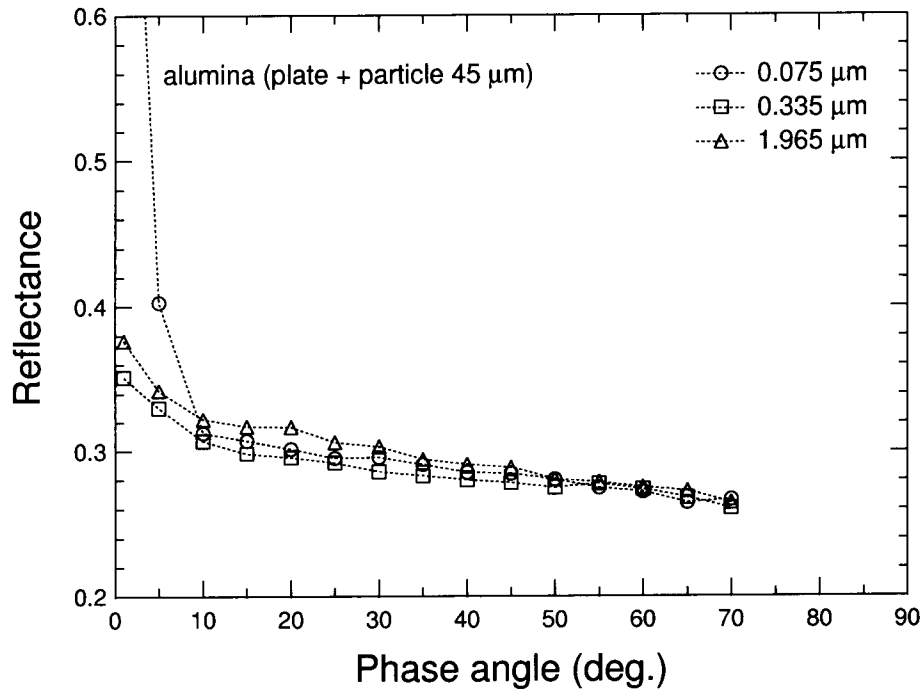

Fig. 3.6. Backscattering reflectance as a function of incident angle for alumina particle with diameter of 0.1μm on plates with different surface roughness.
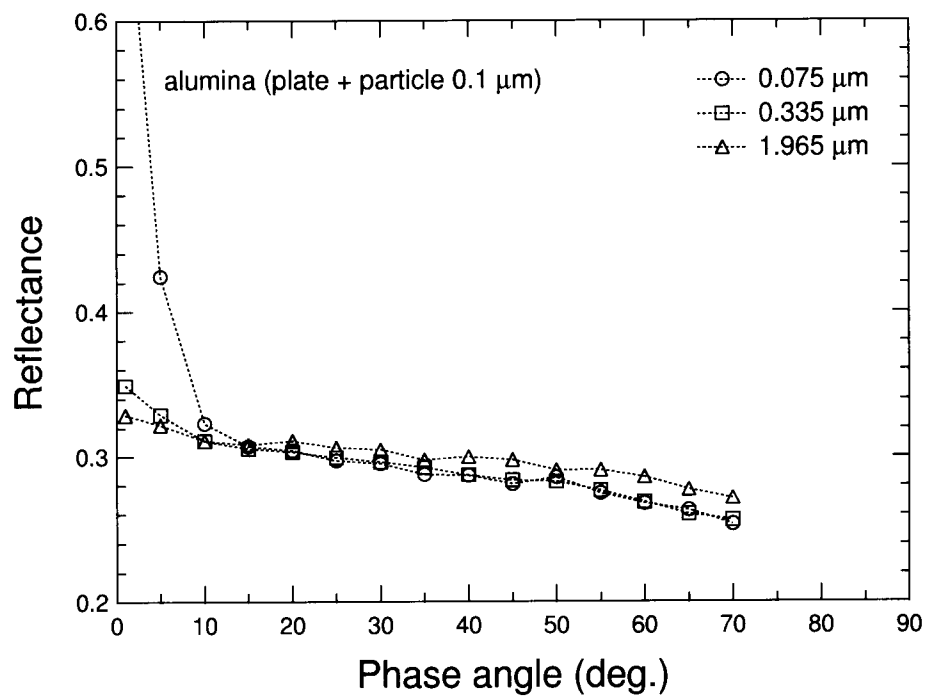
15

Fig. 3.7. Bidirectional reflectance as a function of phase angle for alumina plates with different surface roughness.

Fig. 3.8. Bidirectional reflectance as a function of phase angle for alumina particles with different diameter.

16

Fig. 3.9. Bidirectional reflectance as a function of phase angle for alumina particle with diameter of 45 μm on plates with different surface roughness.

Fig. 3.10. Bidirectional reflectance as a function of phase angle for alumina particle with diameter of 0.1 μm on plates with different surface roughness.

17

3.5 Summary and discussions

We performed laboratory measurements of light scattering properties by rough surfaces. The samples used for our measurements are different types of surfaces consisting of alumina (Al_2O_3) plates, particles, and combinations of both.

We investigated the incident angle dependence of backscattered light at small phase angle. The reflected light from the plates covered by the thin layer of the particles has an effect of Fresnel specular reflection by the plates at small incident angle, while depending on the roughness, and decreases as the incident angle. If a regolith exists on an asteroid surface with a thickness much larger than 100 μm, a case not studied here, we think that the brightness of the asteroid surface at small phase angle may be relatively independent of incident angle. The phase angle dependence of scattered light at normal incidence was also investigated. Although the existence of a thin layer of the particles has an effect of diluting Fresnel specular reflection by the plate, a nonlinear increase by the particulate layer, called the opposition effect, is added at small phase angles. As expected, the effect of Fresnel specular reflection is strongest in case of the smoothest plate and weaker as the plate is rougher. The absolute reflectance of 45 μm particle layer is stronger than those of 500 μm and 0.1 μm particle layers. It may be caused by the effect of the single-scattering albedo and the phase function of the individual particles or the porosity of the particle layer.

For future works, we are planning to measure backscattered light properties of regolith layers by changing the wavelength of light, the thickness of particulate layer, and using various different samples, *i.e.* optical constants, size and shape of particles, porosity and so on. Also it is important to compare our results with theoretical models (*e.g.* Iwasaki and Mukai 1999) and observations.

4 On the Asymmetry Parameter of Asteroid Photometric Data: Bidirectional Reflectance of Powdered Samples at Large Phase Angles

4.1 Introduction

Interpretation of the photometric measurements obtained by remote-sensing plays an important role in estimating physical and geological properties of planetary surfaces. The most widely used model in analyzing the photometric data of planetary surfaces with regolith layer, Hapke's bidirectional reflectance model, is an approximate light scattering model from radiative transfer theory (Hapke 1993). The analyses of asteroidal data based on the Hapke's model have retrieved mean particle phase functions having back scattering nature, *i.e.* the asymmetry parameter (or cosine asymmetry factor) being negative (Helfenstein *et al.* 1989). It is well known, on the other hand, that natural soil particles, individually, have forward single scattering nature in general. Therefore, if the light scattered by regolith layer is dominated by the single scattering of the individual particles, the sign of the asymmetry parameter must be positive that is forward scattering.

The question of negative sign of the asymmetry parameter has been studied by numerical and experimental approaches (Hillier 1997, and references therein). Mischenko (1994, 1997) suggested that the apparent back scattering character of planetary regolith particles is an artifact introduced by use of Hapke's bidirectional reflectance model by comparing the Hapke's model with the rigorous numerical solutions of the radiative transfer for independently scattering particles. McGuire and Hapke (1995) and Hapke (1996) showed from both theoretical arguments and experimental data that inhomogeneous composite particles such as rock fragments and agglutinates, which appear to be abundant in planetary regoliths, can account for the back scattering character. Also he pointed out that the approximate light scattering model can correctly retrieve the sign of the asymmetry parameter, if the range of the phase angle covered by the data set is sufficiently large.

Both laboratory measurements of scattered light by particulate surfaces and photometric observations of planetary surfaces for a wide range of phase angle are difficult and limited. However, spacecraft explorations have enabled our access to the data sets with much wider range of the phase angle than we have from the Earth. The Voyager observations of the icy satellites of Uranus and Saturn returned the data with phase angle of $13° - 43°$ for Enceladus, $1.8° - 135°$ for Rhea, $0.8° - 152°$ for Titania, and $12° - 159°$ for Triton. The retrieved asymmetry parameters were all negative, though those obtained from terrestrial snow and frost surfaces were positive. Based on this opposite signs of the asymmetry parameter, Verbiscer and Veverka (1990) suggested that frost grains on icy satellites are aggregated into particles of complex texture.

The recent *in situ* photometry of Gaspra, Ida, and Mathilde also returned the data of wider range of phase angle than the ground-based data (Helfenstein *et al.* 1994, 1996, Clark *et al.* 1999). The phase angle coverage were $33° - 51°$, $19.5° - 109.8°$, and $40° - 136°$. The spacecraft data show back scattering nature; The asymmetry parameters were -0.18 ± 0.04, -0.33 ± 0.01, and -0.25 ± 0.04 respectively, when one-term Henyey-Greenstein phase function is used as the single-scattering particle phase function.

The single-scattering particle phase function behavior of Mathilde is rather better described by the two-term Henyey-Greenstein phase function. The best fit values retrieved from it are $\xi_1 = -0.27 \pm 0.04$, $\xi_2 = 0.66 \pm 0.01$, and $f = 0.24 \pm 0.09$, where ξ_1 and ξ_2 are the respective asymmetry parameters of separate backscattering and forward scattering terms and f is a partition coefficient describing how to linearly combine the two terms. The effective asymmetry parameter ξ_{eff} is then $\xi_{eff} = (1 - f)\xi_1 + f\xi_2 = -0.05$, which is nearly zero.

Helfenstein and Veverka (1989) estimated the Hapke parameters from laboratory photometric data with the phase angle of roughly, $4° - 120°$ for two meteorite powders. Both solutions of the asymmetry parameter were marginally positive or negative, i.e. 0.075 ± 0.016 for a carbonaceous chondrite, Murchison (French 1980) and -0.085 for an ordinary chondrite, Bruderheim (Egan et al. 1973).

In this paper, we present the results of measurements of bidirectional reflectance of powdered surfaces with four different kinds of material, including a carbonaceous chondrite, Allende (CV3) and a ordinary chondrite, Gao (H5). We determined four Hapke parameters from our data for the cases of a wide ($2° - 155°$) and a narrow ($2° - 80°$) range of phase angle. We demonstrate, by real laboratory data, how the retrieved Hapke parameters, especially the asymmetry parameter and the single-scattering albedo characterizing the single scattering properties, are changed depending on the covered range of phase angles.

4.2 Experiments

The bidirectional reflectance of powdered surfaces at different angles were measured using a goniometric photopolarimeter which is introduced in section 2. In this work, the collimated beam diameter is typically about 2 mm. The detector at 545 mm distance from the sample surface is a photomultiplier with sensitive surface of 8 mm in diameter. The solid angle seen by the detector is always larger than the spot size of the light.

The samples prepared for measurements were olivine (Horoman; Forsterite), graphite (purity is 98%), a fresh chip of Allende (CV3) and Gao (H5) meteorite. The olivine, Allende, and Gao meteorite samples were ground with a mortar and pestle. The olivine and graphite powders were wet sieved to size ranges of $45 - 53$ μm and $180 - 212$ μm, while Allende and Gao meteorite powders were dry sieved to size ranges of $45 - 75$ μm and $180 - 500$ μm. The size distributions of all samples shown in Figs. 4.1 − 4.4 were obtained by a laser diffractometer (HELOS & RODOS). Scanning electron micrographs of all samples were acquired (Figs. 4.5(a) − 4.12(a)), which revealed that most particles have irregular shapes.

The powders were gently poured into a sample tray to form an optically thick layer with thickness of 6 mm and macroscopically smooth surface. The porosity of olivine and graphite powders were estimated by measuring the weight versus volume and using the specific gravity; 3.3 g/cm^3 for olivine and 2.2 g/cm^3 for graphite. Figures 4.5(b) − 4.12(b) show the three-dimensional surface structures of all samples examined by a laser confocal displacement meter with the horizontal resolutions of 100 μm (20 mm × 20 mm) and 10 μm (2 mm × 2 mm). The surface roughness R_a introduced in section 2 of the layers of olivine particles ($45 - 53$ μm and $180 - 212$ μm) were calculated. The values R_a derived

Table 4.1 **Table 4.1** Samples and conditions of measurements.

Samples				Measurements			
Material	Refractive index	Size (diameter)	Porosity	i	e	g	Position angle
olivine (Mg$_2$SiO$_4$)	$n = 1.68$ $k = 0.0001$ (at 0.62 μm)	45 − 53 μm	0.54	75°	−73° ∼ 80°	2° ∼ 155°	0° ↓ 90° ↓ 180° ↓ 270°
				0°	2° ∼ 80°	2° ∼ 80°	
		180 − 212 μm	0.47	75°	−73° ∼ 80°	2° ∼ 155°	
				0°	2° ∼ 80°	2° ∼ 80°	
graphite (C)	$n = 2.6$ $k = 1.2$ (at 0.63 μm)	45 − 53 μm	0.75	75°	−73° ∼ 80°	2° ∼ 155°	
				0°	2° ∼ 80°	2° ∼ 80°	
		180 − 212 μm	0.67	75°	−73° ∼ 80°	2° ∼ 155°	
				0°	2° ∼ 80°	2° ∼ 80°	
Allende (CV3) meteorite	-	45 − 75 μm	-	75°	−73° ∼ 80°	2° ∼ 155°	
				0°	2° ∼ 80°	2° ∼ 80°	
		180 − 500 μm	-	75°	−73° ∼ 80°	2° ∼ 155°	
				0°	2° ∼ 80°	2° ∼ 80°	
Gao (H5) meteorite	-	45 − 75 μm	-	75°	−73° ∼ 80°	2° ∼ 155°	
				0°	2° ∼ 80°	2° ∼ 80°	
		180 − 500 μm	-	75°	−73° ∼ 80°	2° ∼ 155°	
				0°	2° ∼ 80°	2° ∼ 80°	

from the three-dimensional structure with the vertical resolution of 0.1 μm and the horizontal resolution of 10 μm are 29.9 μm for 45 − 53 μm particles and 86.8 μm for 180 − 212 μm particles, which are about the half of the individual particle size.

We measured the bidirectional reflectance of these samples under the conditions of two ranges of phase angle. One is wide coverage of phase angle, from 2° to 155°, at 75° incident angle and the other is narrow coverage, from 2° to 80°, at 0° incident angle. We assured especially for the measurement of large phase angle that the detected light is the reflected light from the sample surface, not the scattered light from any obstacles along the beam path between the sample and the laser, as follows. We performed a measurement without the sample tray but an another tray with a hole at its center. The laser beam passed through the hole and we detected no significant increase of the signal from the dark level: the dark level is detected by shutting off the beam by a chopper in front of the laser window. The reflectance was calibrated using the standard white surface made by Ba$_2$SO$_4$ as described in section 2. In order to even the inhomogeneity of the sample surface illuminated by the laser beam and the laser speckle patterns, the sample tray was rotated by 90° step, *i.e.* the position angles of the tray were 0°, 90°, 180°, and 270°. All samples and conditions of measurements are summarized in Table 4.1.
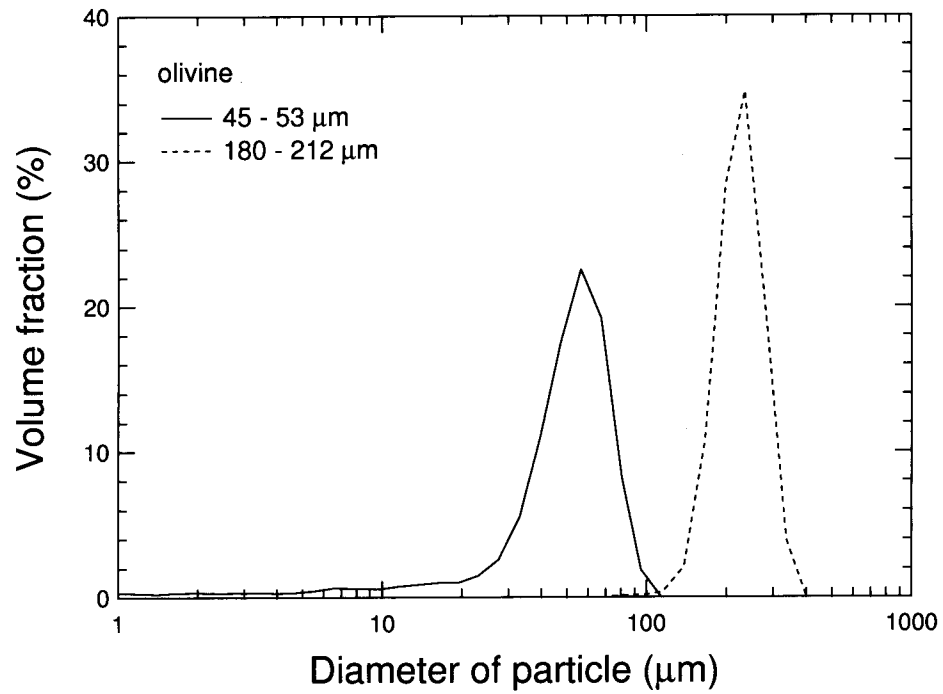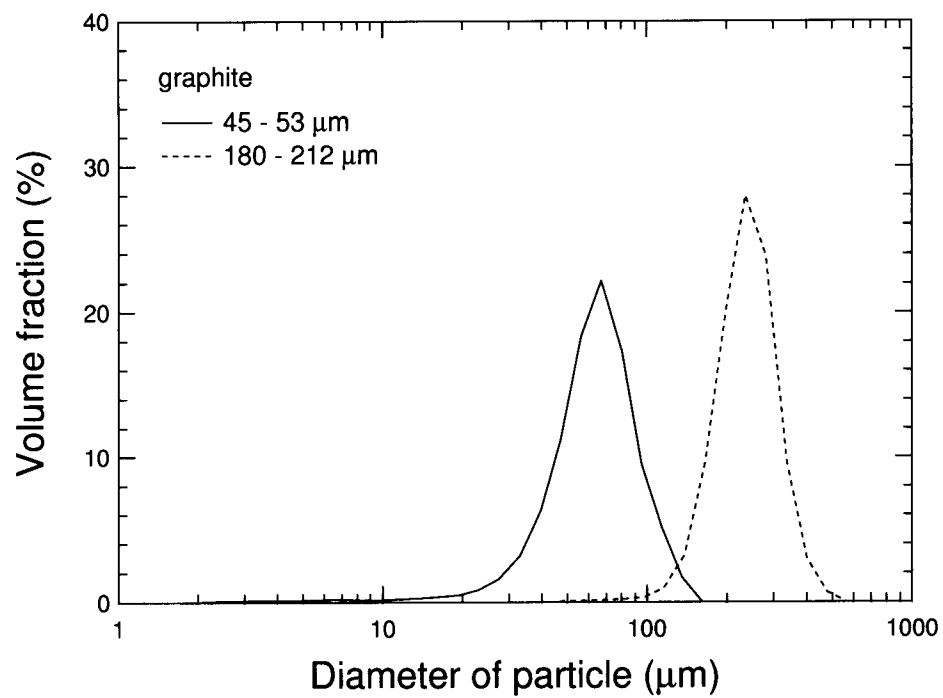
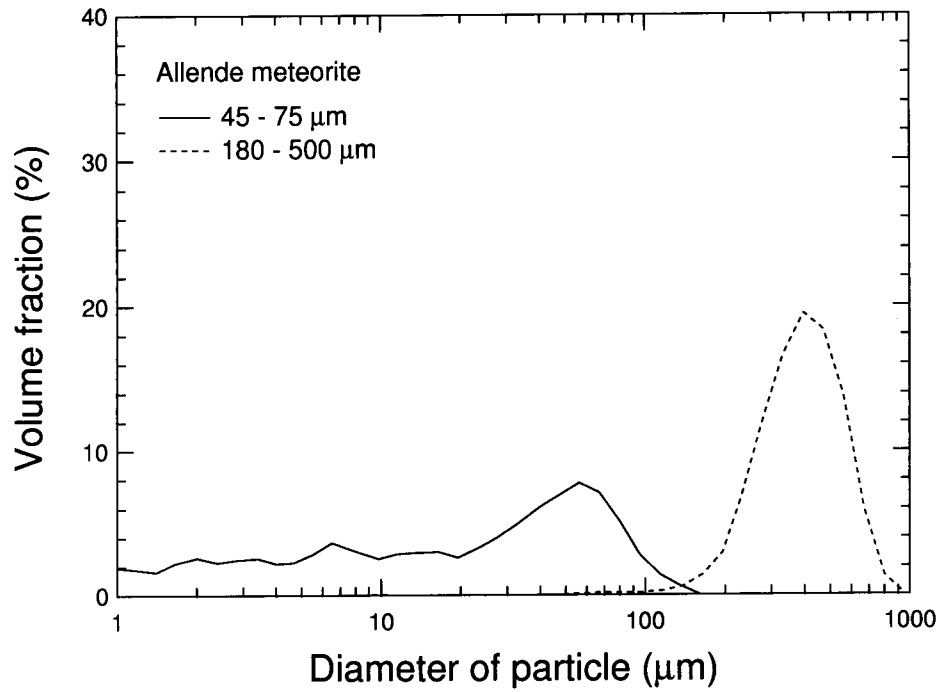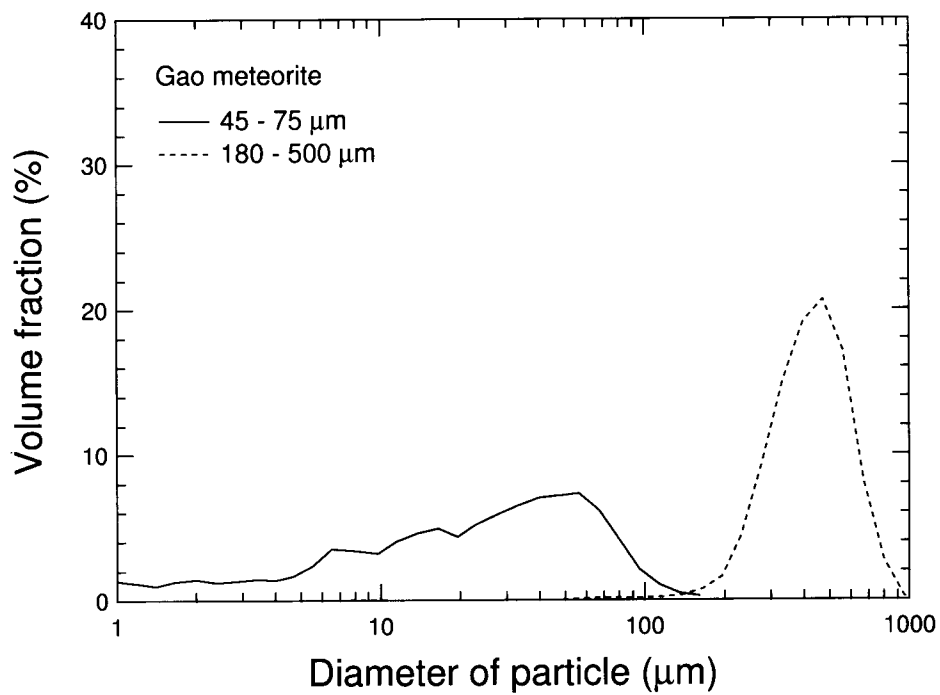**Fig. 4.1.** Size distributions of olivine particles.

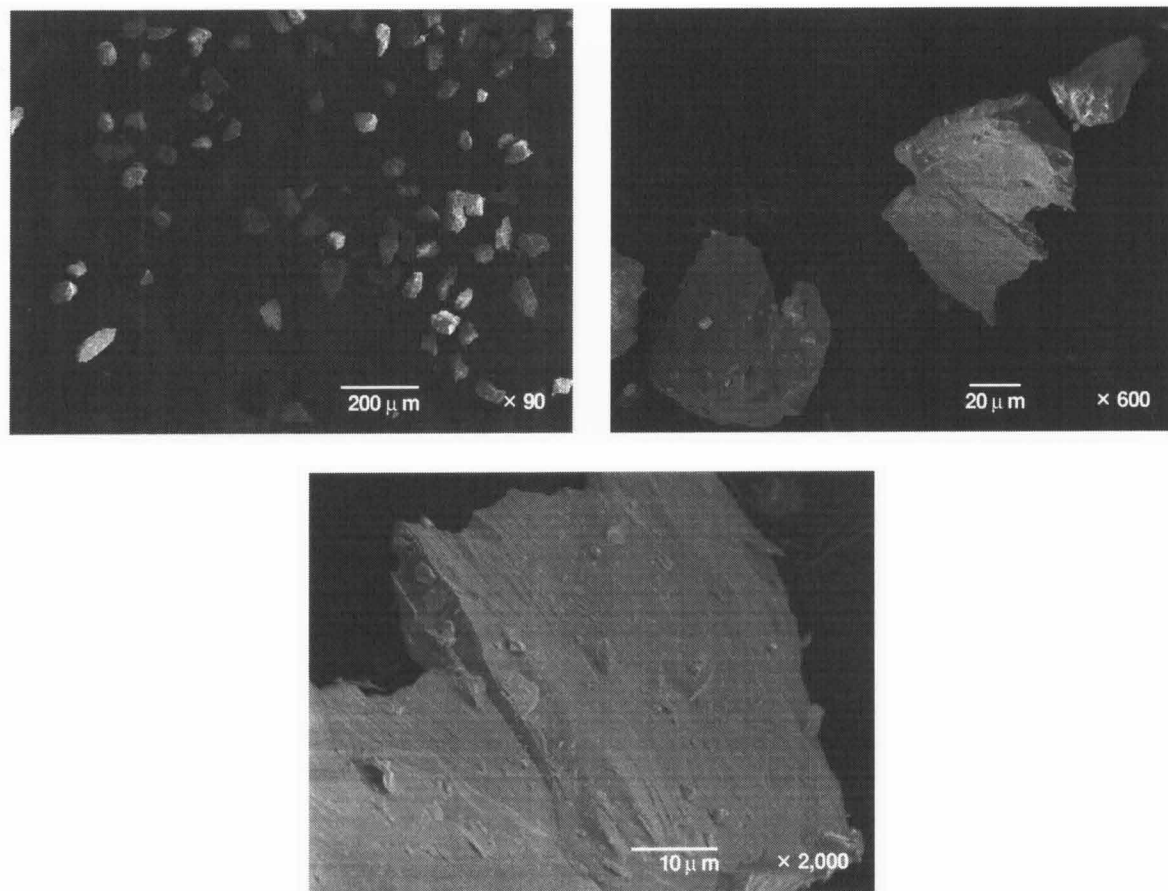**Fig. 4.2.** Size distributions of graphite particles.

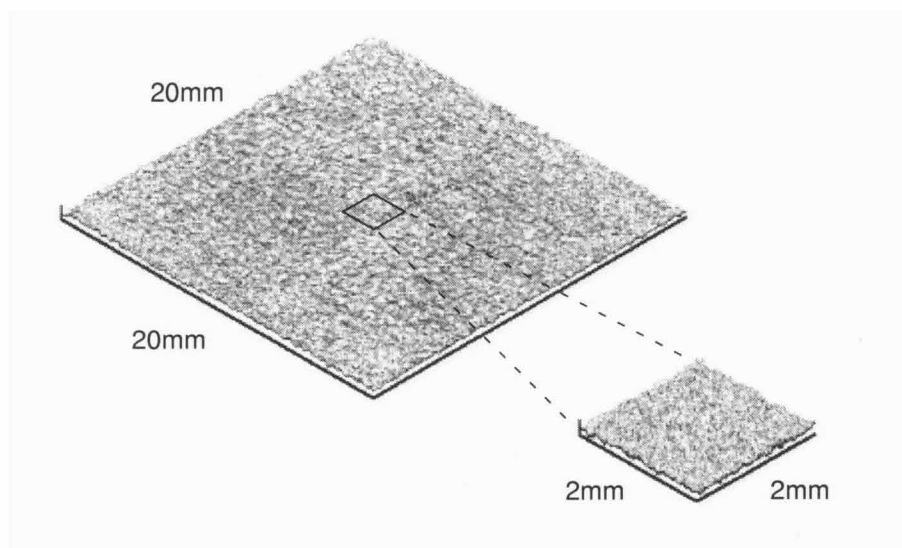**Fig. 4.3.** Size distributions of Allende meteorite particles.

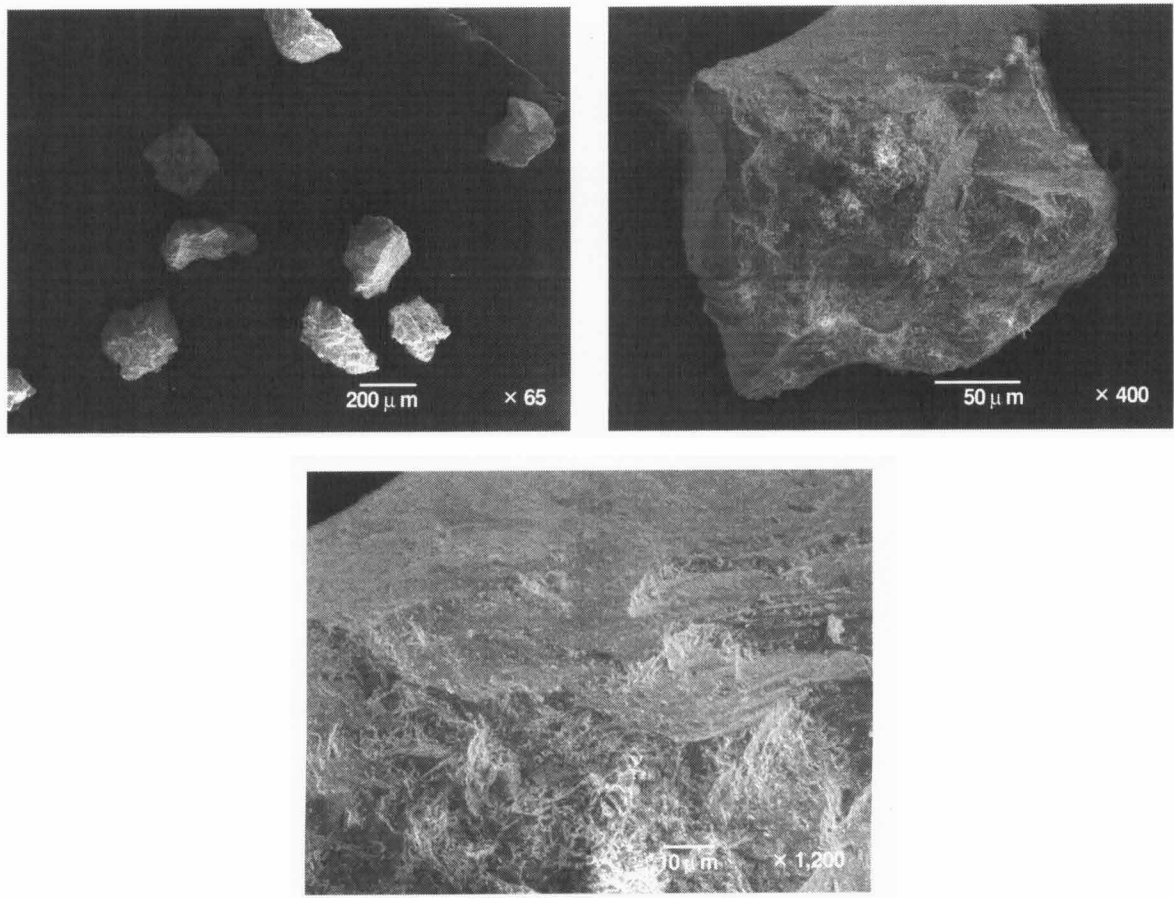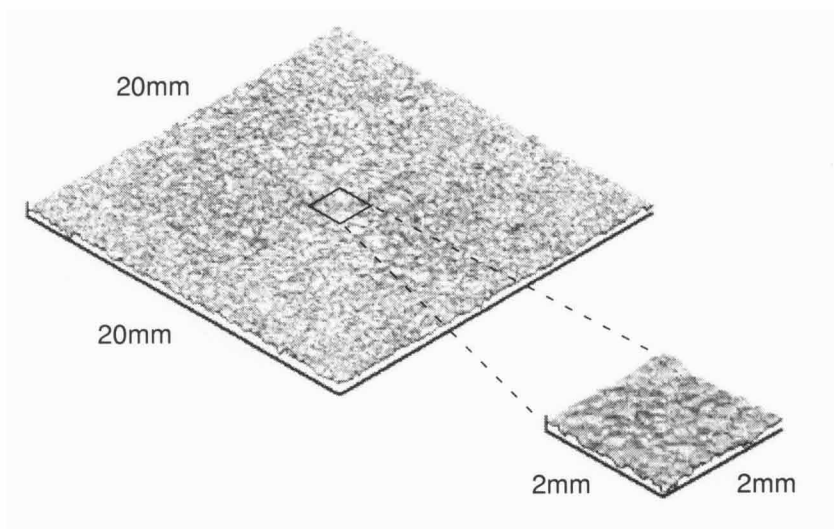**Fig. 4.4.** Size distributions of Gao meteorite particles.

(a)

(b)

Fig. 4.5. Electron photomicrograph (a) and three-dimensional surface structure of a layer (b) of olivine particles $(45 - 53\ \mu\text{m})$.
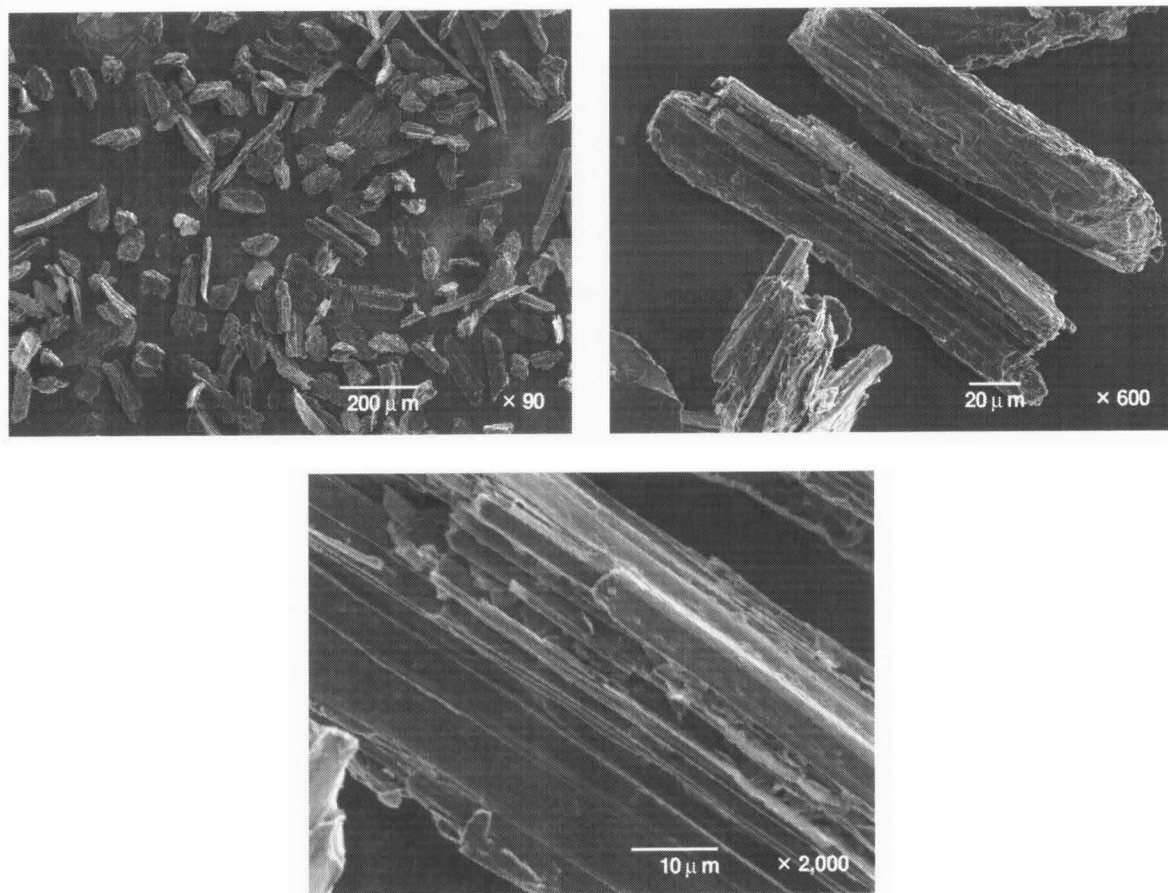
(b)

Fig. 4.6. Electron photomicrograph (a) and three-dimensional surface structure of a layer (b) of olivine particles ($180 - 212$ μm).

25

(a)

(b)

Fig. 4.7. Electron photomicrograph (a) and three-dimensional surface structure of a layer (b) of graphite particles ($45 - 53$ μm).
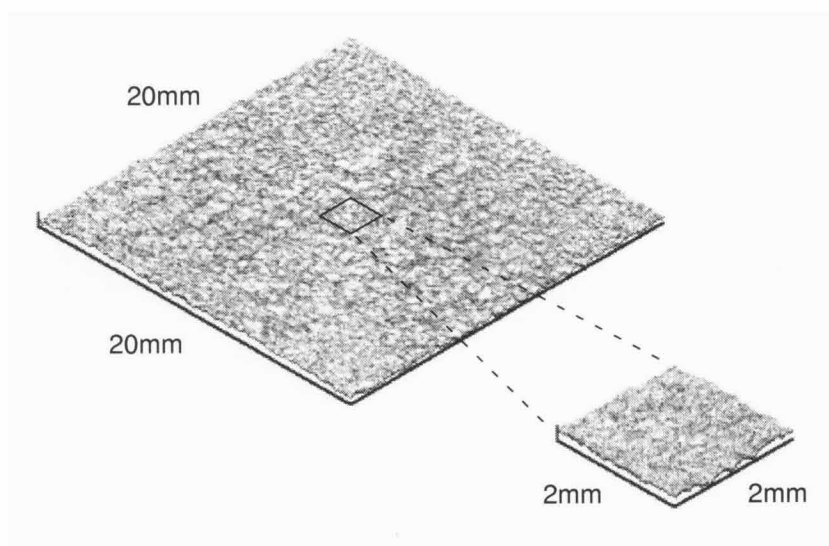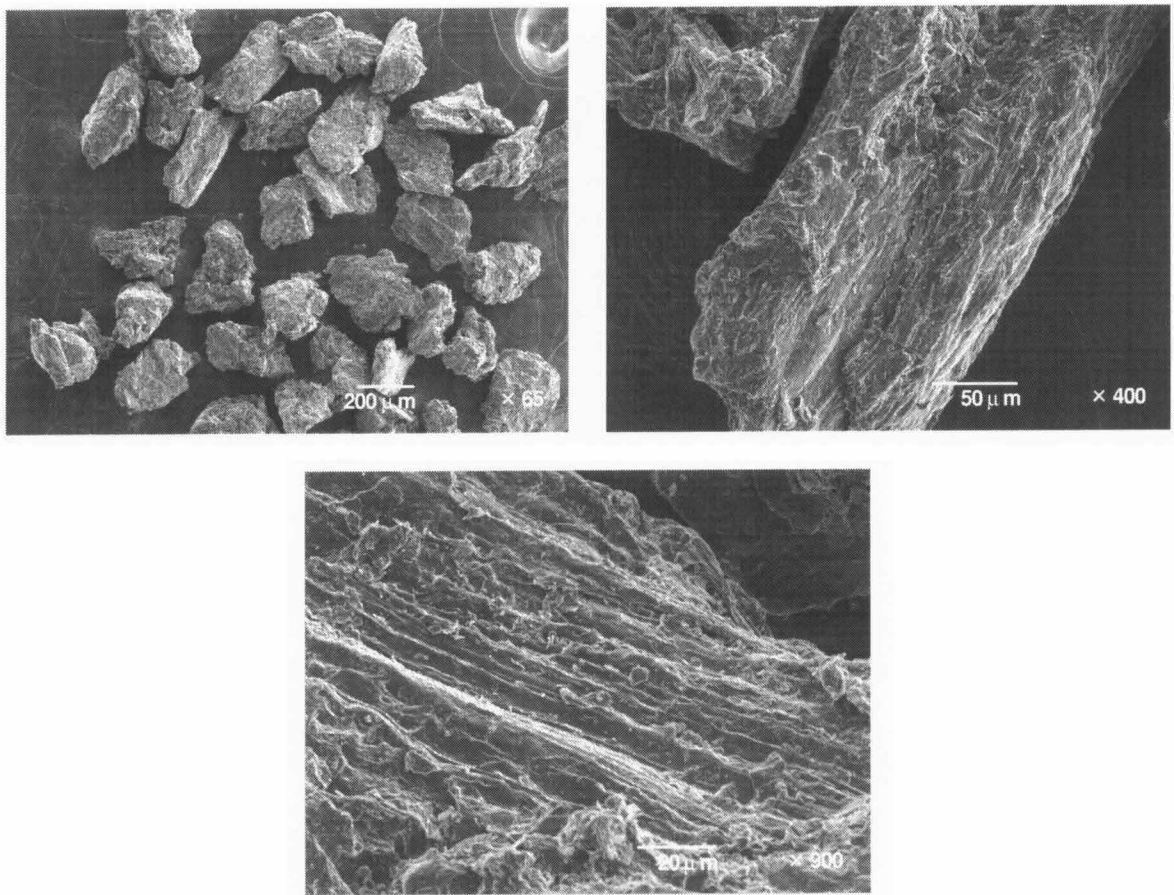
(a)

(b)

Fig. 4.8. Electron photomicrograph (a) and three-dimensional surface structure of a layer (b) of graphite particles $(180 - 212 \ \mu\text{m})$.

(a)

(b)

Fig. 4.9. Electron photomicrograph (a) and three-dimensional surface structure of a layer (b) of Allende meteorite particles ($45 - 75$ μm).

28

(a)

(b)

Fig. 4.10. Electron photomicrograph (a) and three-dimensional surface structure of a layer (b) of Allende meteorite particles (180 − 500 μm).
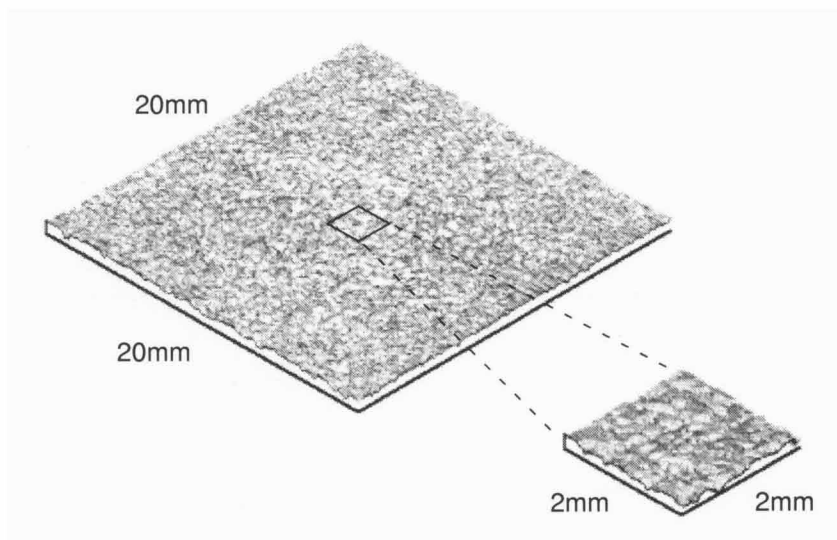
29

(a)

(b)

Fig. 4.11. Electron photomicrograph (a) and three-dimensional surface structure of a layer (b) of Gao meteorite particles ($45 - 75$ μm).

(a)
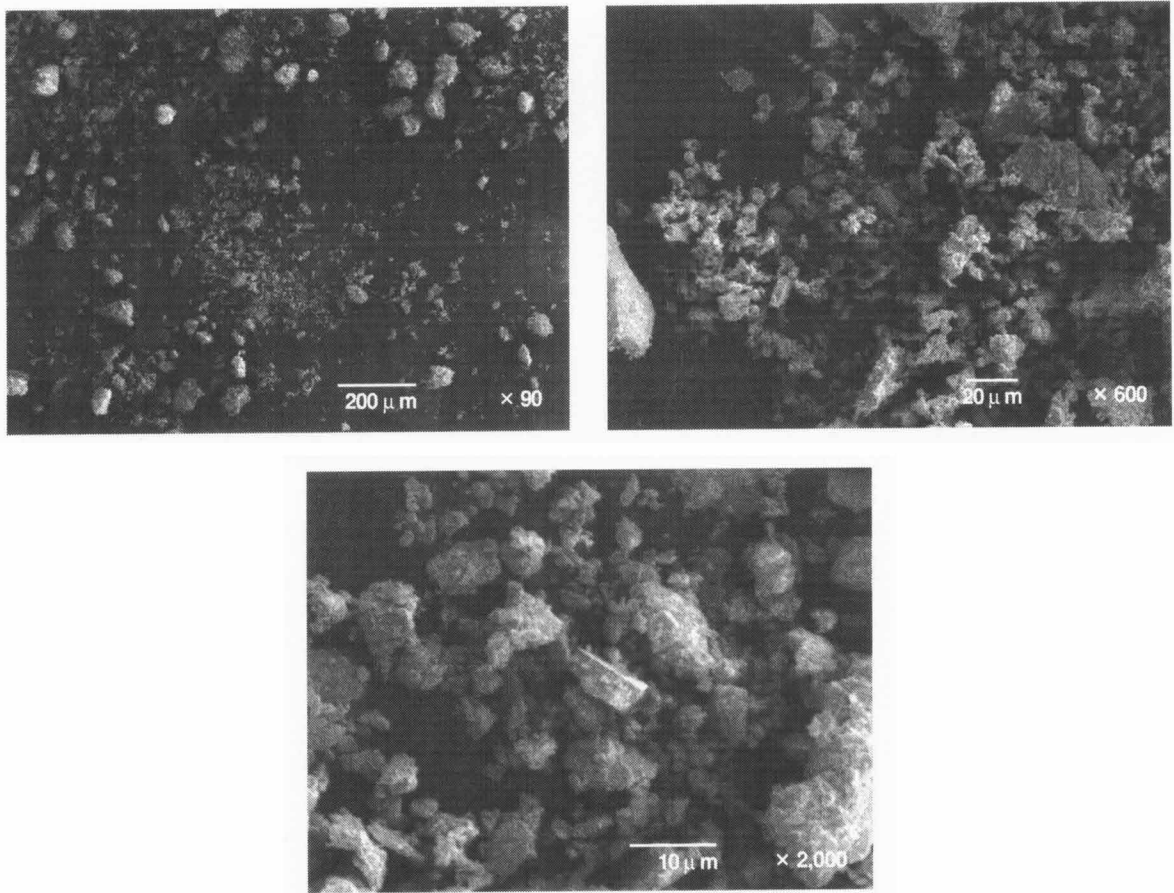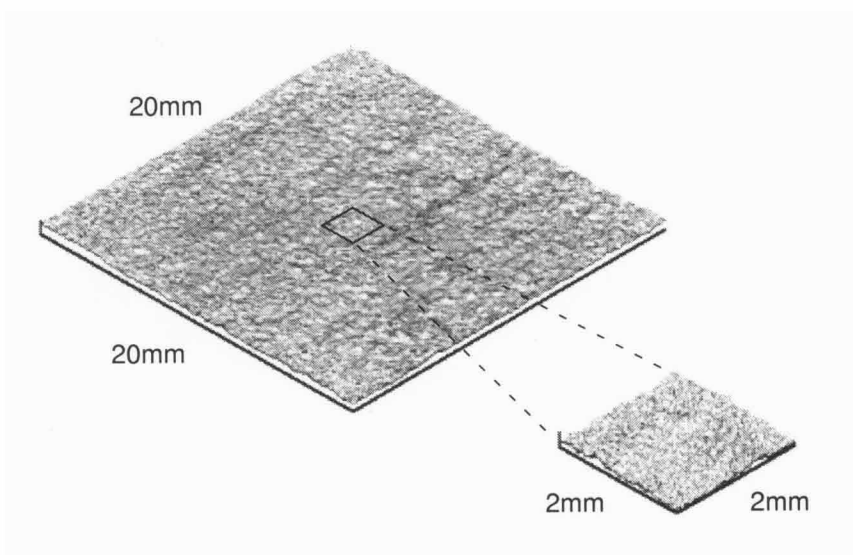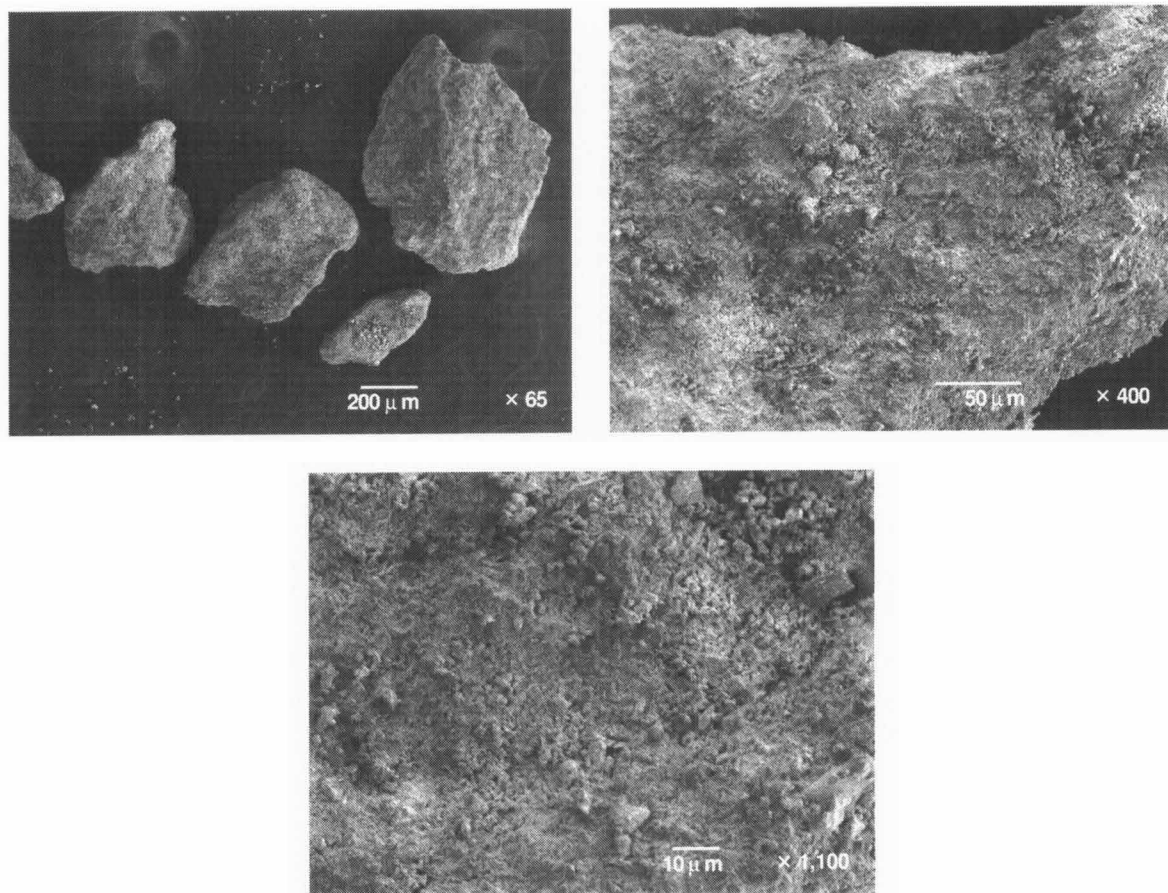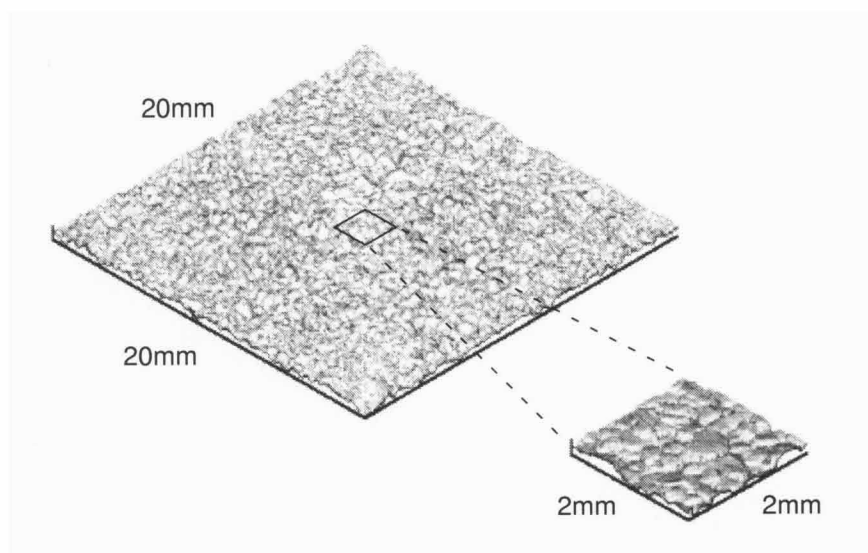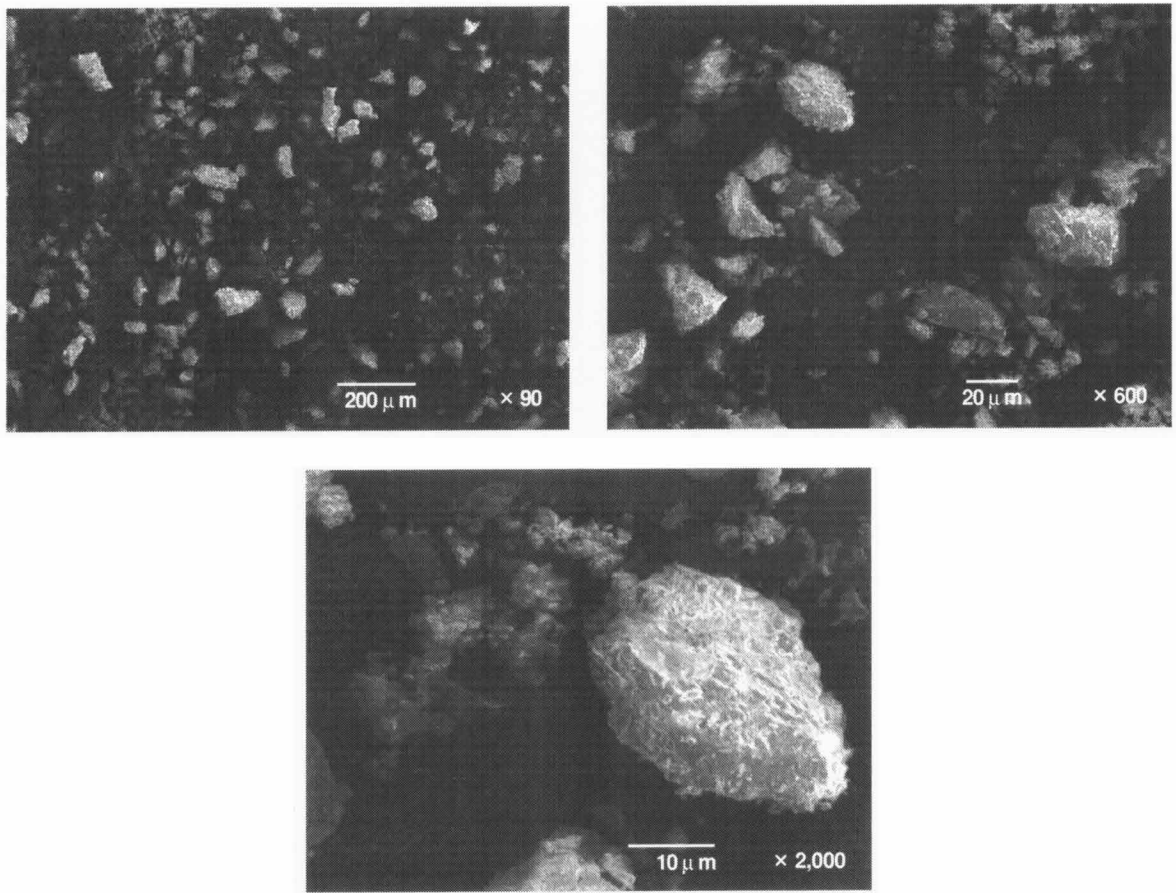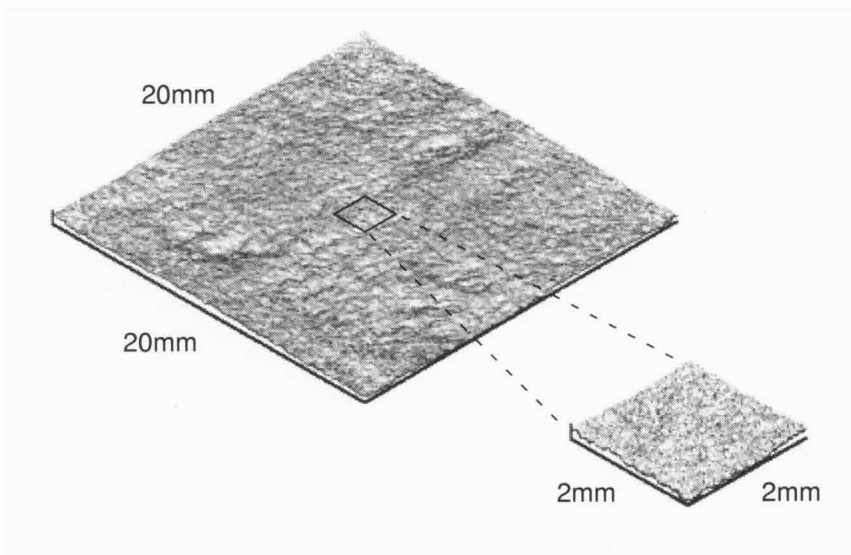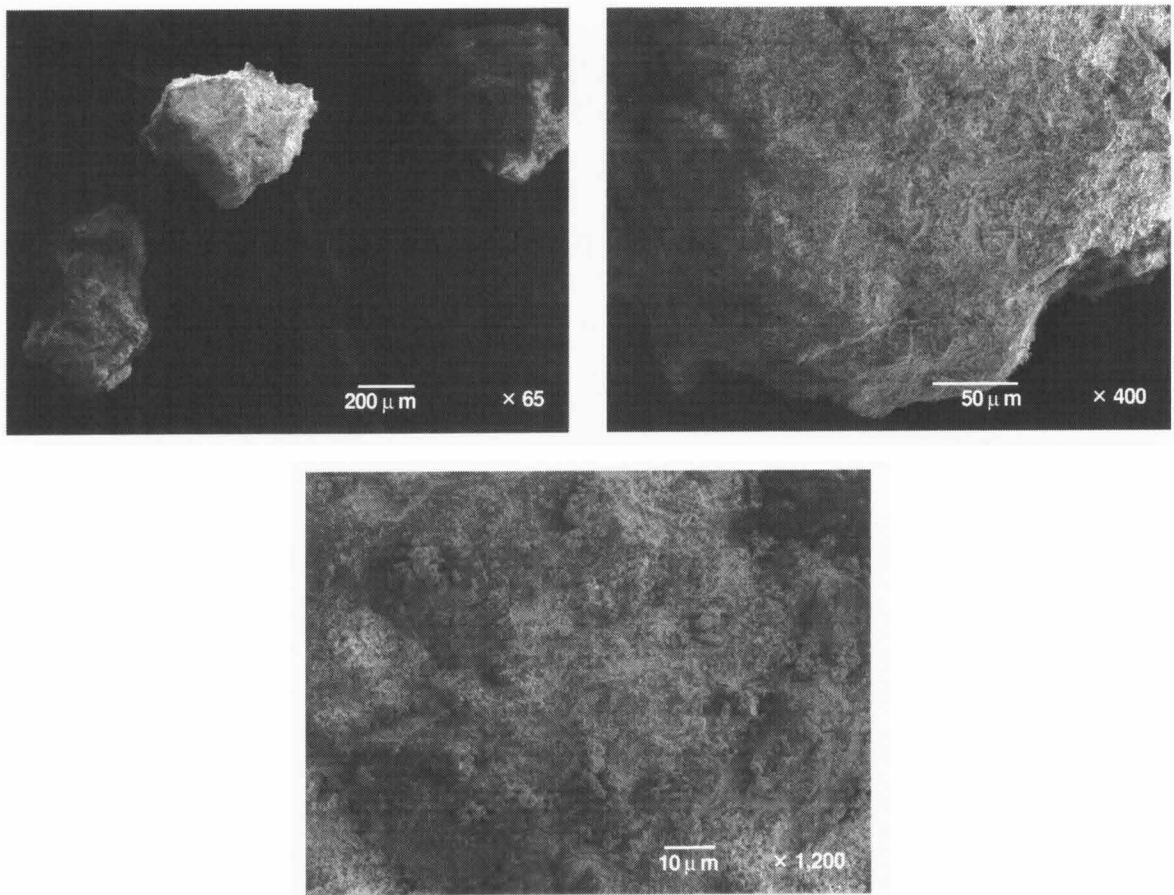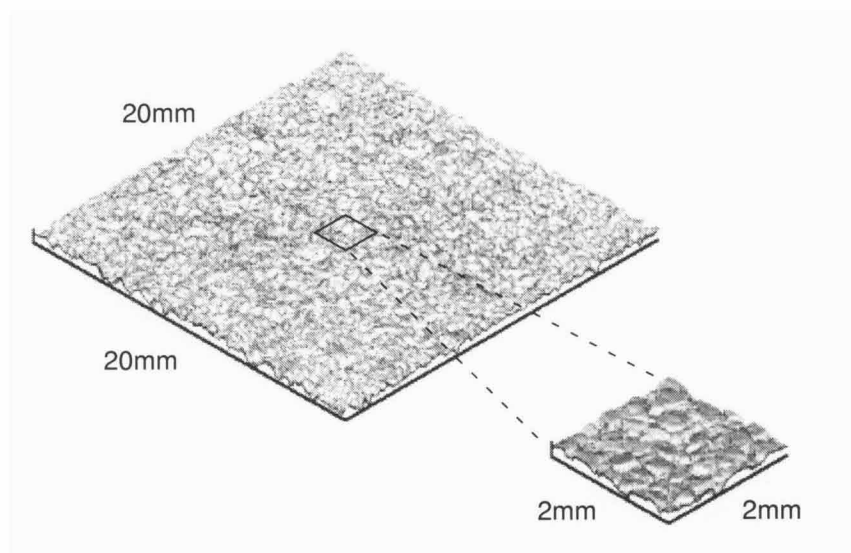

(b)

Fig. 4.12. Electron photomicrograph (a) and three-dimensional surface structure of a layer (b) of Gao meteorite particles ($180 - 500$ μm).

4.3 Hapke's bidirectional reflectance model

Theoretical and experimental works show that significant information for the surface structure of solar system bodies can be derived from the observations of their bidirectional reflectance. Hapke's bidirectional reflectance model is widely used in planetary photometry to describe the scattering of light from rough, particulate surfaces, and for relating photometric behavior to physical and geological properties of the surface terrains. In this model, the contribution from singly scattered rays is derived exactly. The opposition effect is assumed to be due to interparticle shadow hiding, in which shadows cast by particles upon one other disappear near opposition, and is derived by an approximation to the Seeliger-Irvine formulation, with significant differences that allow for a size distribution of particle and also include a more rigorous derivation of the extinction, scattering, and absorption coefficients. The multiple scattering contribution is calculated from a modified two-stream solution of the radiative transfer equation for isotropic scatterers and with a collimated source.

The bidirectional reflectance of a particulate medium is defined as the ratio of the scattered radiance at the detector to the incident irradiance. Since particulate layers used for our measurements are macroscopically smooth surfaces, the equation is

$$r(i,e,g) \;=\; \frac{\omega}{4\pi}\frac{\mu_0}{\mu_0 + \mu}\left\{[1 + B(g)]p(g) + H(\mu_0)H(\mu) - 1\right\}$$

$$B(g) \;=\; \frac{B_0}{1 + (1/h)\tan(g/2)}$$

where i denotes the zenith angle of incidence, e is the zenith angle of emergence, g is the phase angle, $\mu_0 = \cos i$, and $\mu = \cos e$. The geometry and nomenclature that will be used in this paper are defined in Fig. 4.13. The adequacy of this approximation clearly depends on the single-scattering albedo and the degree of nonisotropy of the scatterers. The approximation would be poor for a medium consisting of large, weakly absorbing, isolated particles, which have strong diffractive forward scattering. However, in planetary regoliths and laboratory powders the diffractive term is absent, some absorption is invariably present, and the irregular shapes and presence of internal scatterers cause the particle phase function to be fairly isotropic. For these materials this approximation should be reasonably accurate.

Hapke's bidirectional reflectance model for smooth surface requires at least four Hapke parameters: the single-scattering albedo ω, the opposition surge angular width h, the opposition surge amplitude B_0, and the asymmetry parameter ξ. The asymmetry parameter is defined as the average value of the cosine of the scattering angle:

$$\xi \;=\; \langle\cos\theta\rangle \;=\; \frac{1}{2}\int_0^\pi \cos\theta\, p(\theta)\sin\theta\, d\theta$$

$$=\; -\langle\cos g\rangle \;=\; -\frac{1}{2}\int_0^\pi \cos g\, p(g)\sin g\, dg$$

where θ is the scattering angle, $i.e.$ $\theta = \pi - g$, and $p(\theta)$ is the single-scattering particle phase function. Theoretically, the asymmetry parameter can be vary from -1 to $+1$ and

i : zenith angle of incidence
e : zenith angle of emergence
g : phase angle
ψ : azimuth
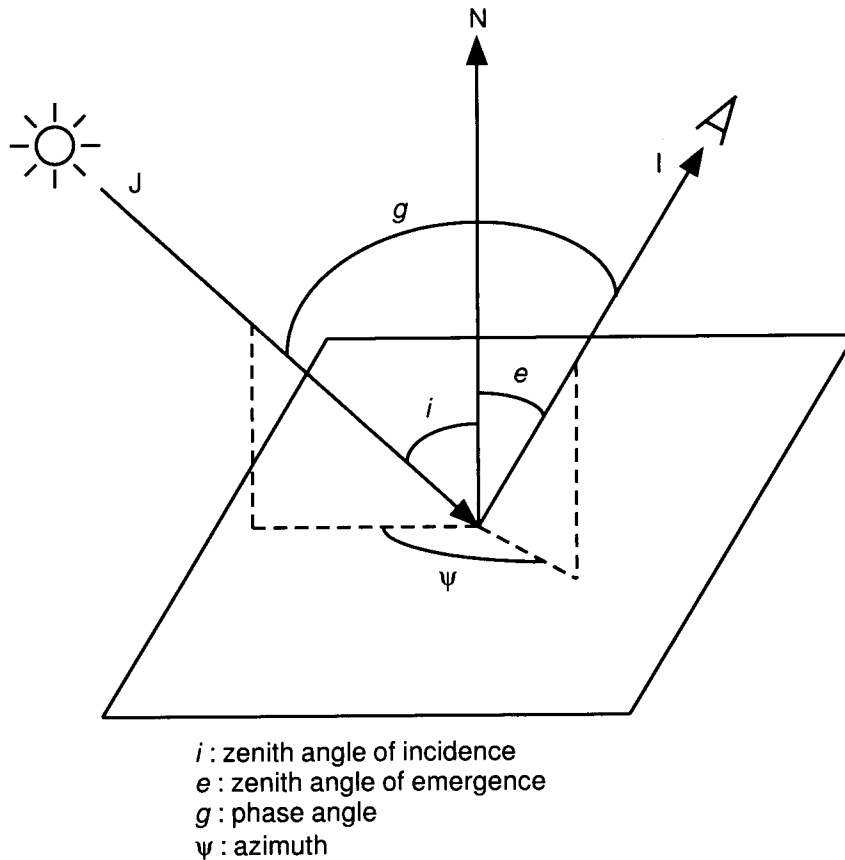
Fig. 4.13. Schematic diagram of bidirectional reflectance, showing the various angles.

is negative for backscattering grains, positive for forward scattering grains, and zero for isotropic scatterers. Hapke parameters for selected small bodies derived by previous work, including macroscopic roughness for rough surface model, were shown in Table 4.2.

4.4 Results and discussions

The results of measurements are shown in Figs. 4.14 − 4.21, where the bidirectional reflectance are plotted as a function of phase angle. The error bars represent standard deviations (1σ) between the data at different position angles, *i.e.* dominant errors are due to the inhomogeneity of the samples in the beam. For all samples, the reflectance shows the opposition effect. As phase angle increase, the bidirectional reflectance gradually decrease and then increase from about 100° for the measurements of the wider range of phase angle, showing forward scattering lobes. The differences in the reflectance between olivine and Gao meteorite particles with different size distributions is obvious. The reflectance of the smaller particles is higher than that of the larger particles. However, there is no distinct difference in reflectance between the particles with different size distributions of dark materials, such as graphite and Allende meteorite particles. NEAR observations indicated that Mathilde's surface has lack of significant reflectance variations. The results here shows the difficulty of detecting the regolith size variation on such low albedo asteroid

Table 4.2 Hapke parameters of selected small bodies.

Object	Data	Phase	Single scattering albedo ω	Opposition surge width h	Opposition surge amplitude B_0	Asymmetry parameter ξ	Macroscopic roughness $\bar{\theta}$
Moon[a]	DI	$0° - 150°$	0.21	0.07	2.01	−0.10	20.0°
	DR	$-124.5° - +135°$ $(g_{min} = -2.3°)$					
		(Dark terrains)	0.12	0.12	1.16	−0.14	8.10°
		(Average terrains)	0.25	0.06	1.84	−0.11	20.6°
		(Bright terrains)	0.33	0.05	1.83	−0.09	24.0°
Avg C-type[b]		$< 25°$	0.037 ± 0.003	0.025 ± 0.001	1.03 ± 0.01	-0.47 ± 0.01	(20°)
Avg S-type[b]		$< 25°$	0.23 ± 0.02	0.020 ± 0.001	1.32 ± 0.03	-0.35 ± 0.01	(20°)
Mathilde[c]	DR	$40° - 140°$	0.0035	0.074	3.18	−0.25	19°
Ceres[b]	DI	$1° - 22°$	0.057 ± 0.004	0.059 ± 0.006	1.58 ± 0.01	-0.40 ± 0.01	(20°)
Vesta[b]	DI	$2° - 25°$	0.40 ± 0.03	0.044 ± 0.010	1.03 ± 0.10	-0.30 ± 0.03	(20°)
Apollo[b,h]	DI	$0° - 89°$	0.318 ± 0.004	0.034 ± 0.007	0.90 ± 0.02	-0.32 ± 0.01	$15° \pm 1°$
Ida[d]	DI	$1° - 121°$	$0.218^{+0.024}_{-0.005}$	0.020 ± 0.005	1.53 ± 0.10	-0.33 ± 0.01	$18° \pm 2°$
	DR	$20° - 110°$					
Dactyl[d]	DR	$20° - 26°$	$0.211^{+0.028}_{-0.010}$	[0.020]	[1.53]	-0.33 ± 0.01	$23° \pm 5°$
Gaspra[e]	DI	$2° - 25°$	0.360 ± 0.07	0.060 ± 0.01	1.63 ± 0.07	-0.18 ± 0.04	$29° \pm 2°$
	DR	$33° - 51°$					
Toutatis[f]	DI	$0° - 121°$	0.261 ± 0.019	0.036 ± 0.023	1.20 ± 0.32	-0.29 ± 0.06	$32° \pm 8°$
Castalia-N[g]	DI	$58° - 90°$	0.384 ± 0.07	-	-	-0.11 ± 0.09	$46° \pm 10°$
Castalia-S[g]	DI	$58° - 90°$	0.239 ± 0.07	-	-	-0.30 ± 0.09	$25° \pm 10°$
Themis[h]	DI	$0° - 21°$	0.048	0.060	1.6	−0.40	5°
Nysa[h]	DI	$0° - 22°$	0.58	0.0055	0.6	−0.40	27°
Hesperia[h]	DI	$0° - 16°$	0.154	0.036	0.94	−0.40	35°
Alkmene[h]	DI	$2° - 27°$	0.183	0.047	1.4	−0.28	5°
Cyrene[h]	DI	$0° - 13°$	0.204	0.022	1.19	−0.383	10°
Aurelia[h]	DI	$1° - 15°$	0.204	0.030	0.47	−0.60	25°
Phobos[i]	DR	$1° - 123°$	0.054	0.072	5.7	−0.13	21°
Deimos[j]	DR	$1° - 81°$	0.079	0.068	1.65	−0.29	16.4°
Mercury[h]	DI	$2° - 123°$	0.21	0.030	1.85	−0.40	20°

Note. DI, Disk-integrated; DR, Disk-resolved.

[a] Helfenstein *et al.* 1987

[b] Helfenstein and Veverka 1989

[c] Clark *et al.* 1999

[d] Helfenstein *et al.* 1996

[e] Helfenstein *et al.* 1994

[f] Hudson and Ostro 1998

[g] Hudson *et al.* 1997

[h] Bowell *et al.* 1989

[i] Simonelli *et al.* 1998

[j] Thomas *et al.* 1996

surface even if the difference *did* exist, for example between the vicinity of fresh craters and other places.

We determined four Hapke parameters from our data by applying weighted nonlinear least-squares fitting, which minimize the summed squares of differences between laboratory data r_n and those retrieved from Hapke's equation $r(i, e, g, \omega, h, B_0, \xi)$. When laboratory errors σ_n are given, it is best to seek parameters which minimize χ^2, defined as

$$\chi^2 = \sum_n \frac{\left[r_n - r(i, e, g, \omega, h, B_0, \xi)\right]^2}{\sigma_n^2} .$$

The model curves of these parameters are shown by broken line in Figs. 4.14 − 4.21 and the retrieved Hapke parameters are listed in Table. 4.3. Here we used the one-term Henyey-Greenstein phase function as the single-scattering particle phase function:

$$p(g) = \frac{1 - \xi^2}{(1 + 2\xi \cos g + \xi^2)^{3/2}}$$

and the approximated H functions for the isotropic scattering function:

$$H(x) = \left[1 - \left(1 - \sqrt{1 - \omega}\right)x\left\{r_0 + \left(1 - \frac{1}{2}r_0 - r_0 x\right)\ln\frac{1 + x}{x}\right\}\right]^{-1}$$

$$r_0 = \frac{2}{1 + \sqrt{1 - \omega}} - 1 .$$

The sign of the asymmetry parameter for most samples change from negative to positive, when the measured range of phase angle is widen from $2° - 80°$ to $2° - 155°$. However, the sign of the asymmetry parameter for larger particles of Allende and Gao meteorite remain negative, but closer to zero than that for smaller particles. The single-scattering particle phase functions of olivine and graphite particles derived from the asymmetry parameter are much different from those calculated by Mie theory using the meaured size distributions, which is the exact solutions of light scattering for a spherical particle (Figs 4.22 and 4.23). There is no distinct difference between the values of single-scattering albedo retrieved from two ranges of phase angle. The values of the single-scattering albedo of our samples are large compared with those derived for asteroids. Although C-chondrite is a candidate for the surface material of C-type asteroids, the single-scattering albedo retrieved from our graphite ($\omega = 0.20 \sim 0.24$) or Allende meteorite data ($\omega = 0.21 \sim 0.27$) is large compared with those for Ceres ($\omega = 0.057$) or Mathilde ($\omega = 0.0035$) (Helfenstein *et al.* 1989, Simonelli *et al.* 1999). The reason of the discrepancy has not been clarified yet.

Although not all the variety of particle type has been investigated, the scattering properties of the particles shown here should be representative of those of typical particles

35

**Table 4.3** Hapke parameters retrieved from our laboratory data.

Samples		Geometry			Hapke parameters			
Material	Size (diameter)	i	e	g	ω	h	B_0	ξ
olivine (Mg2SiO4)	45 − 53 μm	75°	−73° ∼ 80°	2° ∼ 155°	0.74	0.016	1.39	0.10
		0°	2° ∼ 80°	2° ∼ 80°	0.72	0.003	1.29	−0.35
	180 − 212 μm	75°	−73° ∼ 80°	2° ∼ 155°	0.61	0.179	0.76	0.08
		0°	2° ∼ 80°	2° ∼ 80°	0.61	0.002	2.23	−0.27
graphite (C)	45 − 53 μm	75°	−73° ∼ 80°	2° ∼ 155°	0.21	0.173	2.64	0.19
		0°	2° ∼ 80°	2° ∼ 80°	0.24	0.004	2.08	−0.30
	180 − 212 μm	75°	−73° ∼ 80°	2° ∼ 155°	0.23	0.069	1.16	0.00
		0°	2° ∼ 80°	2° ∼ 80°	0.20	0.094	0.69	−0.25
Allende (CV3) meteorite	45 − 75 μm	75°	−73° ∼ 80°	2° ∼ 155°	0.23	0.120	5.77	0.19
		0°	2° ∼ 80°	2° ∼ 80°	0.27	0.032	1.37	−0.21
	180 − 500 μm	75°	−73° ∼ 80°	2° ∼ 155°	0.21	0.045	2.51	−0.09
		0°	2° ∼ 80°	2° ∼ 80°	0.22	0.042	1.94	−0.20
Gao (H5) meteorite	45 − 75 μm	75°	−73° ∼ 80°	2° ∼ 155°	0.49	0.108	2.35	0.08
		0°	2° ∼ 80°	2° ∼ 80°	0.48	0.054	0.75	−0.24
	180 − 500 μm	75°	−73° ∼ 80°	2° ∼ 155°	0.34	0.029	1.59	−0.17
		0°	2° ∼ 80°	2° ∼ 80°	0.32	0.040	1.22	−0.27

in planetary regoliths. From our laboratory results we confirm that the one-term Henyey-Greenstein phase function, which is the most common empirical function used in single scattering modeling, is not capable of describing the scattering behavior of particulate surfaces made of anisotropically scattering material which simultaneously displays significant forward and backward scattering components. However, most planetary data sets do not contain observations in both forward and backward scattering directions. Most disk-integrated data of planetary surfaces are restricted to phase angle of < 30°, where no information in the forward scattering direction is available. Because there is no information to accurately constrain a multiparameter single-scattering particle phase function in such data, the one-term Henyey-Greenstein phase function may be appropriate. On the other hand, the disk-resolved data or laboratory data contain information in the forward scattering direction, it is desirable to use the two-term Henyey-Greestain phase function, which can be describe both components of light scattering. The sign of the asymmetry parameter for larger particles of Allende and Gao meteorite remain negative, even though the coverage of phase angle is wider. This fact may indicate that the reason why the sign of the asymmetry parameter previously derived from the *in situ* observational data are not positive values, is that the regolith particles of asteroids have meteorite like materials and larger particles (hundreds micron in size).

Further laboratory and *in situ* observational investigations are required for determining asteroid surface composition and texture from bidirectional reflectance.
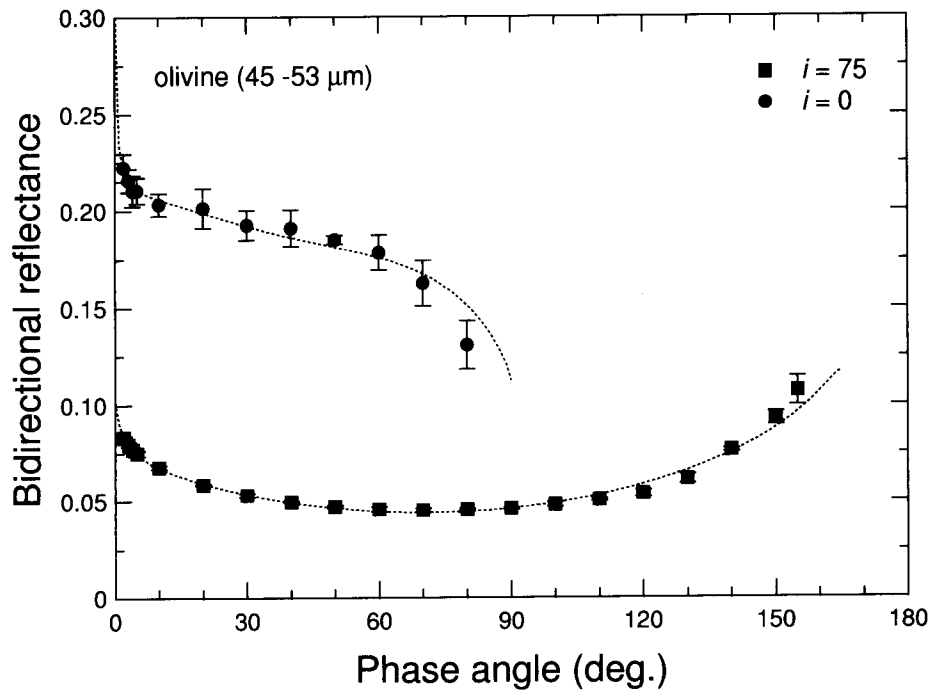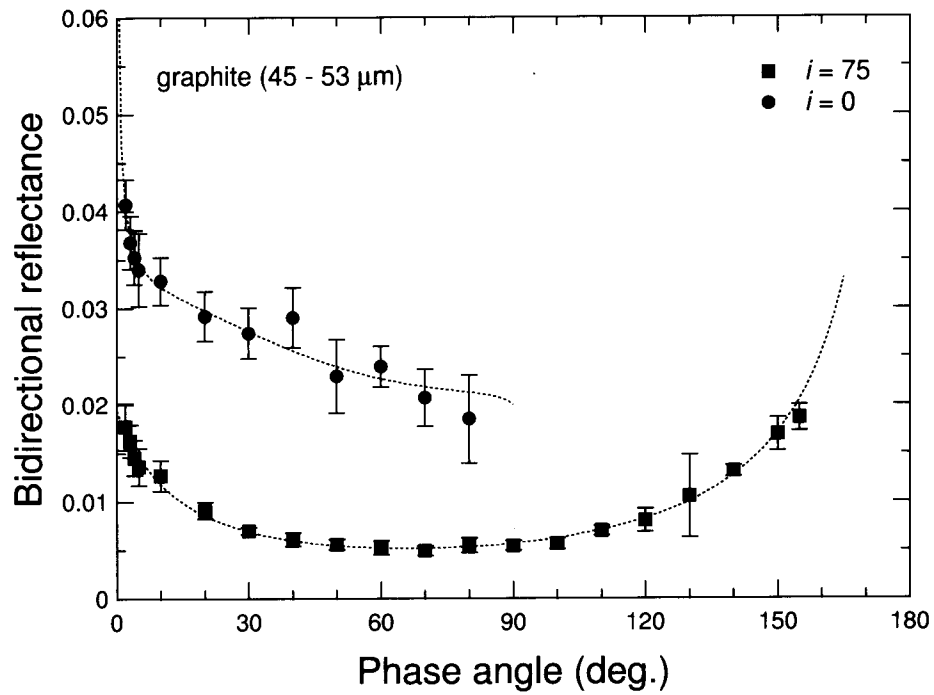
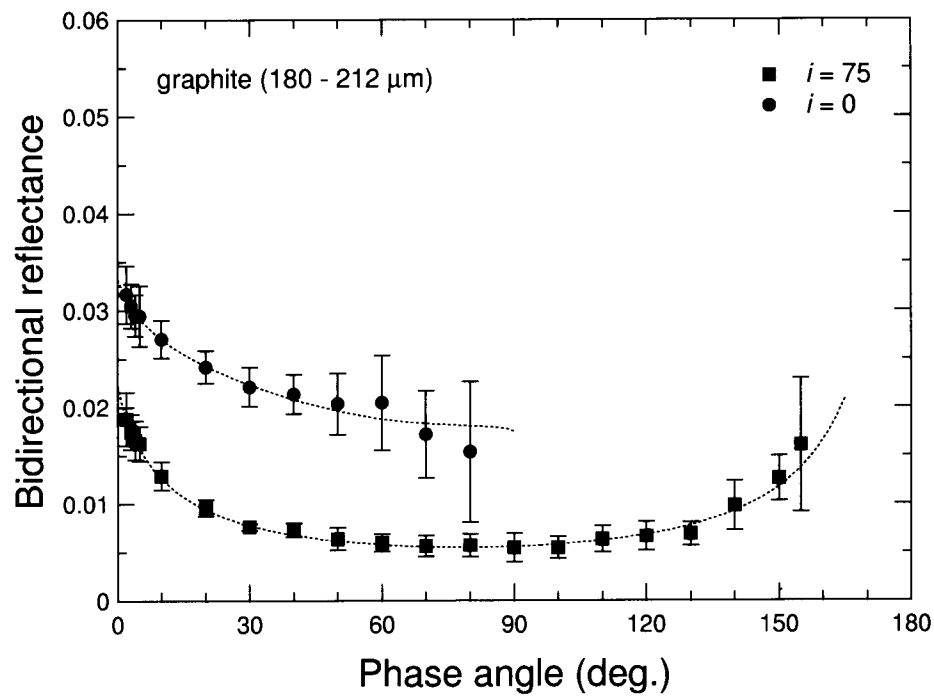**Fig. 4.14.** Bidirectional reflectance as a function of phase angle for olivine samples (45 − 53 μm).
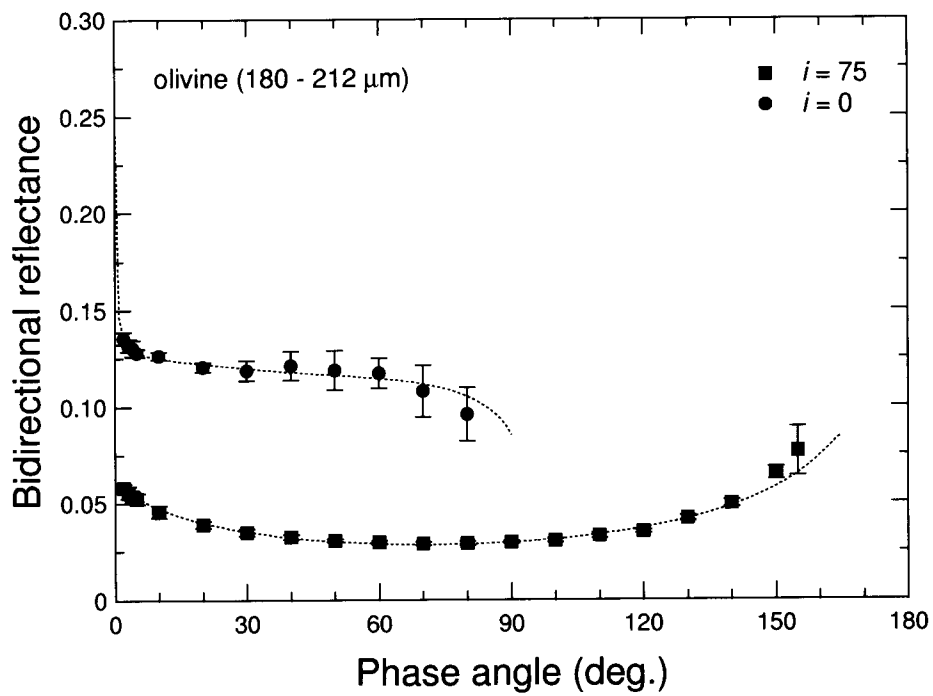
Fig. 4.15. Bidirectional reflectance as a function of phase angle for olivine samples (180 − 212 μm).

37
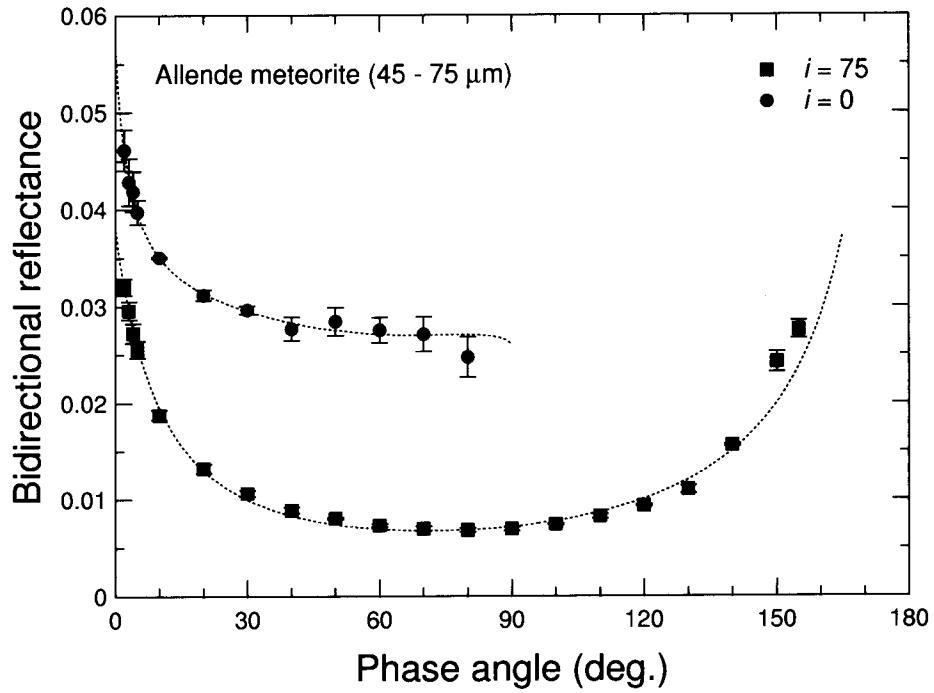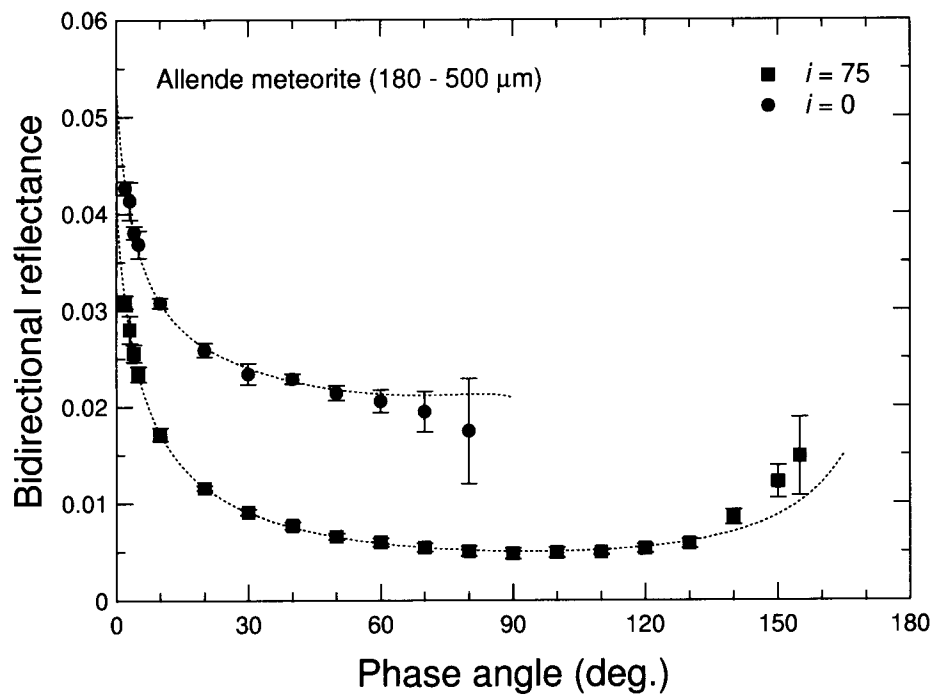
Fig. 4.16. Bidirectional reflectance as a function of phase angle for graphite samples (45 − 53 μm).
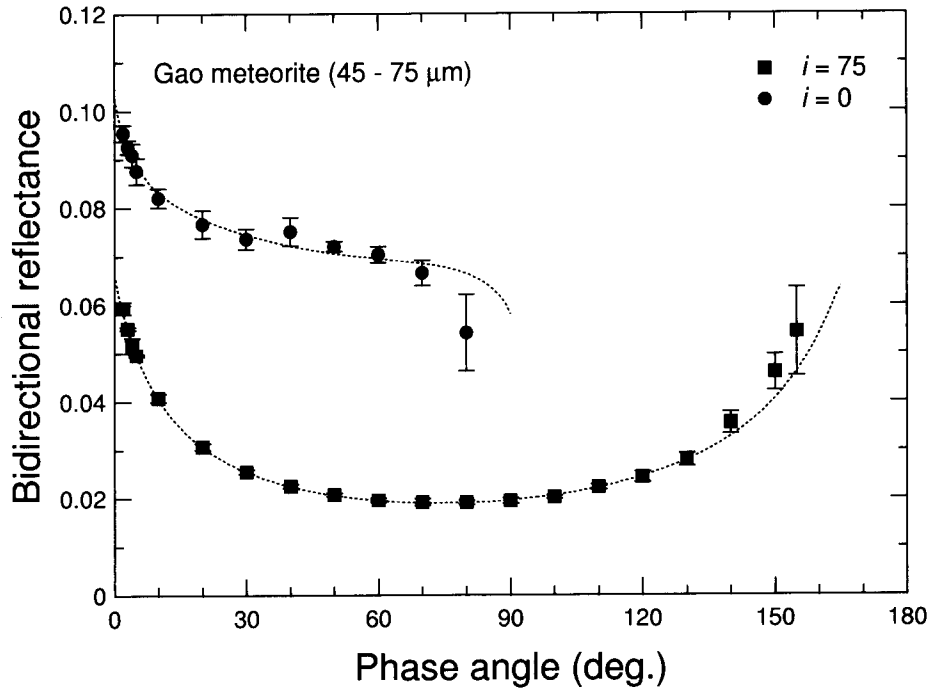

Fig. 4.17. Bidirectional reflectance as a function of phase angle for graphite samples (180 − 212 μm).

Fig. 4.18. Bidirectional reflectance as a function of phase angle for Allende meteorite samples (45 − 75 μm).

Fig. 4.19. Bidirectional reflectance as a function of phase angle for Allende meteorite samples (180 − 500 μm).

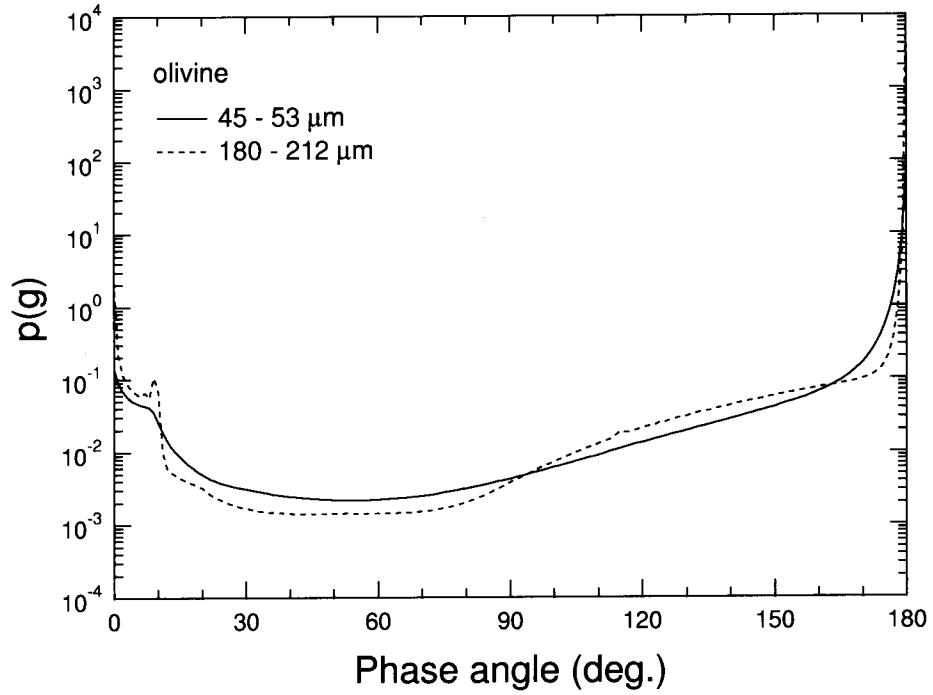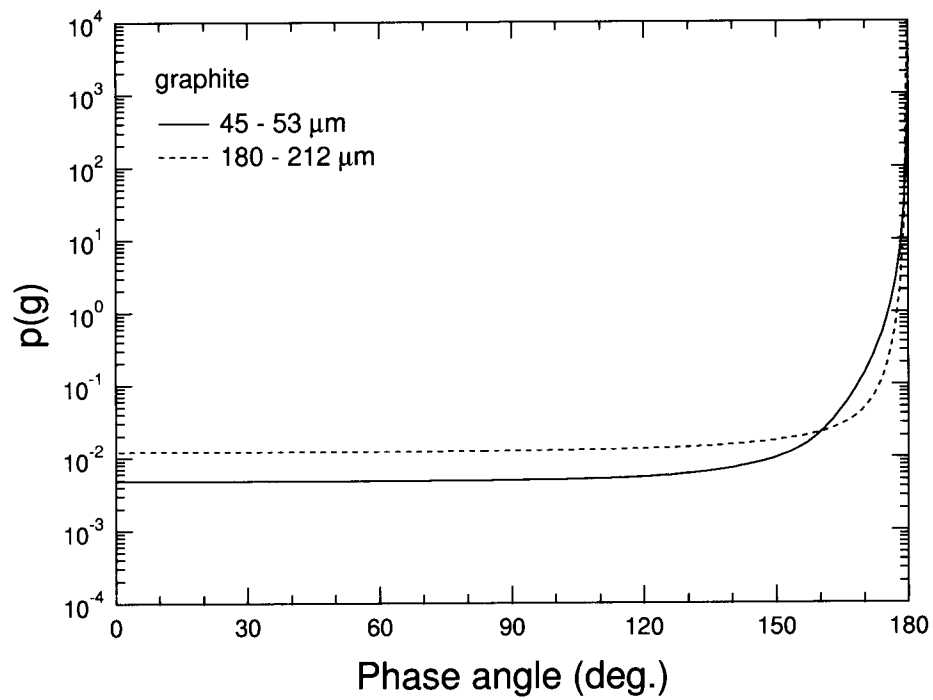**Fig. 4.20.** Bidirectional reflectance as a function of phase angle for Gao meteorite samples (45 − 75 μm).
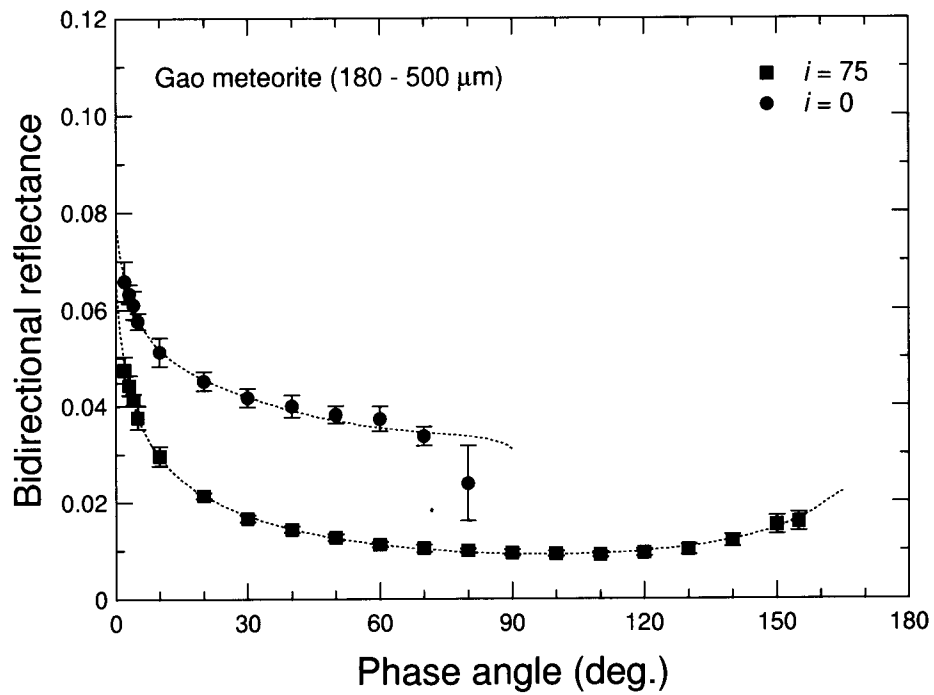
Fig. 4.21. Bidirectional reflectance as a function of phase angle for Gao meteorite samples (180 − 500 μm).

**Fig. 4.22.** Single-scattering particle phase functions of olivine particles calculated by Mie theory.

Fig. 4.23. Single-scattering particle phase functions of graphite particles calculated by Mie theory.

5 Estimation of Asteroid Surface Properties from Polarization-Phase Curve Parameters

5.1 Introduction

In recent years, the *in situ* observations of small bodies in the solar system have been done by space missions and we have obtained detailed information on surfaces of their bodies. The Japanese mission for asteroid sample return (MUSES-C) launched in 2002 will carry a CCD camera (AMICA) to return images of the target asteroid. Visible photo-polarimetry will be performed by this camera and measurements of linear polarization with different phase angles is planned. The main use of the polarization data obtained for planetary surfaces has been for estimating the physical properties of such surfaces, *i.e.* surface texture and optical properties. Previous ground-based observations and laboratory measurements of terrestrial rocks and meteorite samples have demonstrated that small bodies in the solar system are covered with regolith layers with diameters from few tens to hundreds micrometers. Although a general theory of polarization-phase behavior is lacking, numerous laboratory studies have empirically demonstrated that polarization-phase curve parameters are related to surface albedo and texture (Geake and Dollfus 1986).

However the observation geometry is limited to smaller phase angle from ground-based measurements of asteroids, the *in situ* measurements of the target asteroid by MUSES-C will enable us to obtain the data with a wider range of phase angle. The other merit of the *in situ* measurements is the capability of obtaining the disk-resolved polarization data. The texture of the asteroid surface should vary with the local geology, and the *in situ* high-resolution photo-polarimetry can reveal the relation between the texture and the geology. It may be difficult for the AMICA observation, however, to determine the maximum polarization at large phase angle due to the limitation of the spacecraft operation. The minimum polarization at small phase angle and the inversion angle are also difficult to be determined, because it requires the S/N ratio at least hundreds. Referring to previous observations and laboratory data (Dollfus 1999, Geake and Dollfus 1986, and Shepard and Arvidson 1999) and our laboratory measurements of layers consisting of olivine and graphite particles with different size distributions (Kogachi 1999), we investigated four empirical relationship: (1) the maximum of polarization and the albedo, (2) the slope of the polarization-phase curve and the albedo, (3) the minimum of polarization and the albedo, and (4) the inversion angle and the minimum of polarization. In particular, we concentrated on how the empirical relationship between the slope of the polarization-phase curve, which will be possible to determine from the *in situ* measurements by MUSES-C, and the albedo is dependent of the size distribution of the regolith particles. The purpose of this work is to find suitable conditions of the observation and the best choice of polarization-phase curve parameter for estimating the surface properties of the target asteroid from the planned polarimetric observations by MUSES-C, which are limited in the coverage of phase angle and the total number of the observations.
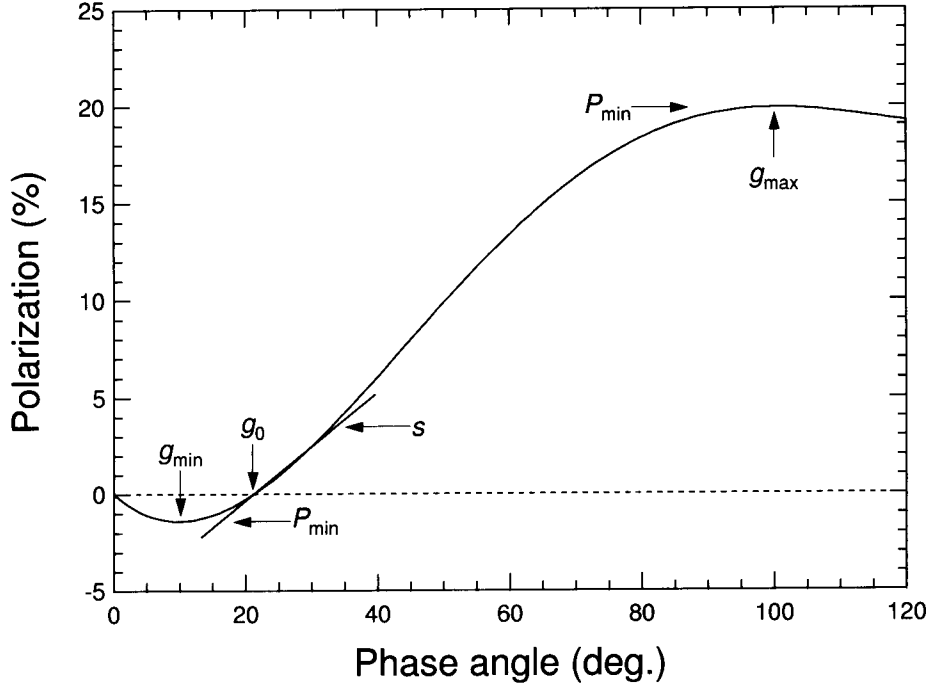
Fig. 5.1. Typical polarization-phase curve for a rough surface, showing how polarization varies with phase angle, and defining the parameters used to describe the curve.

5.2 Polarization-phase curve parameters

The principle of the polarization is based on the observation that when unpolarized light is scattered by a rough surface it become partially linearly polarized, and the plane of polarization is usually found to be either perpendicular to the scattering plane containing the incident and observation rays (regarded as positive polarization) or parallel to this plane (regarded as negative). In terms of intensity components $I_\perp$ and $I_\parallel$, respectively measured perpendicular and parallel to the scattering plane, the degree of linear polarization is defined as

$$P = \frac{I_\perp - I_\parallel}{I_\perp + I_\parallel}$$

usually expressed as a percentage. P is found to change with the phase angle between the incident and observation rays, and a plot of P against the phase angle is found to give a curve characteristic of the surface. The degree of linear polarization P is essentially dependent on the phase angle g. It is not a strong function of the zenith angle of incidence i, emergence e, or the azimuth. Figure 5.1 illustrates the typical characteristics of polarization phase curve, which is a signature of a rough, porous, or particulate surface. The curves are described by the following six parameters (1) P_{min}, which is the minimum of polarization, at phase angle g_{min}; (2) the inversion angle g_0, where the polarization changes sign; (3) h, which is the slope of the polarization-phase curve; and (4) P_{max}, which is the maximum of polarization, at phase angle g_{max}.

43

The polarization of light reflected from a rough surface is considered to be related to the physical properties of surface, i.e. the geometric albedo, the size distribution of regolith particles, and the porosity of regolith layer. The geometric albedo defined as the ratio of apparent surface brightness to that of an ideal Lambert screen, located at the same position and oriented perpendicular to the incident light. Traditionally geometric albedos are measured at a phase angle of 5°, which approximates the linear extrapolation of the photometric magnitude-phase relation to zero phase.

5.3 Relationship among polarization-phase curve parameters, albedo, and particle size

For all kinds of natural solid surfaces, the maximum of polarization P_{max} produced around phase angle 100° is related to the albedo A. The relationship between the maximum of polarization and the albedo was analyzed experimentally (Bowell et al. 1973, Geake and Dollfus 1986). The relationship is expressed by

$$\log P_{max} = C_1 \log A + \log C_2 .$$

Recently, it is found that this relationship is dependent of particle size by a comparison of telescopic measurements of lunar surface and laboratory measurements of pulverized rocks, which is shown in Fig. 5.2 (Dollfus 1999). In Fig. 5.3 previous laboratory data of terrestrial rocks and results of our laboratory measurements of olivine and graphite (Kogachi 1999 and the works shown in section 2) are plotted. The maximum of polarization, however, is difficult to be determined by the polarimetric observation by MUSES-C as described in section 5.1.

It was also found empirically that there is a relationship between the slope of the polarization-phase curve s and the albedo A. This relationship, called the slope-albedo law, is considered to be almost independent of grain size and texture, and almost linear (on a log-log scale), except for very dark surfaces with albedos of less than about 5%. The slope of the polarization-phase curve is thus seen to be a useful indicator of the geometric albedo. The relationship can be written

$$\log A = C_3 \log s + \log C_4 .$$

The constants are determined empirically from telescopic observations of the moon, Mercury, etc. or by laboratory measurements of terrestrial, lunar, and meteoritic materials. Zellner et al. (1977) adopted $C_3 = -0.93$ and $C_4 = -1.78$ from high quality data for meteorite samples. Recently, Lupishko and Mohamed (1996) obtained $C_3 = -0.98$ and $C_4 = -1.73$ from new albedo measurements of ground-based radiometric observations, IRAS satellite data, and observations of stellar occultations by asteroids (Fig. 5.4). Because the relationship between the maximum of polarization and the albedo is dependent of particle size, we expected that this relationship should be also dependent of particle size. In Fig. 5.5 previous laboratory data of terrestrial rocks and results of our laboratory measurements of olivine and graphite are plotted. From the present result, the

slope-albedo law is probably dependent of particle size. Even if the albedo of the target asteroid of MUSES-C will be low like C-type asteroid and it is difficult to determine the regolith size from the albedo alone, as shown in section 4, the regolith size may be determined by the slope of the polarization-phase curve.

The negative branch of the polarization-phase curve is produced by the effects of multiple scattering and mutual shadowing between the particles of the complex texture. It is expedient to describe the shape of this negative branch by two parameters: the minimum of polarization P_{min} and the inversion angle g_0. The minimum of polarization is also related to the albedo A. This relationship is almost linear (on a log-log scale), except for very dark surfaces with albedos of less than about 5%, and the equation is

$$\log A = C_5 \log |P_{min}| + \log C_6 .$$

The constants C_5 and C_6 were determined from the approximation of the asteroid albedo being dependent of the parameter P_{min}. The value of C_5 and C_6 were determined to -1.22 and -0.92, respectively, by new albedo measurements of ground-based radiometric observations, IRAS satellite data, and observations of stellar occultations by asteroids as shown in Fig. 5.6 (Lupishko and Mohamed 1996). In Fig. 5.7 previous laboratory data of terrestrial rocks and results of our laboratory measurements of olivine and graphite are plotted. No dependence of particle size is appeared, which may be due to the inaccuracy of polarimetric measurements.

It has been shown that a plot of the minimum of polarization against the inversion angle may be due to the surface texture. Figure 5.8 shows a plot for telescopic observations of asteroid and Fig. 5.9 shows a plot for previous laboratory data of lunar and terrestrial rocks, lunar fines, pulverized rocks and meteorites, dusty lunar rocks, and bulks of basalt. Each sample characterizes a specific point in the diagram. The plots shown in Fig. 5.9 can be mainly separated three types of the surface, *i.e.* dust free rocks (smaller g_0 and $|P_{min}|$), dusty rocks (middle g_0), and fines (larger g_0 and $|P_{min}|$). Also a general trend can be seen that the lower the albedo, the larger the amount of the minimum of polarization. From this result, we will be able to estimate the surface texture of the target asteroid.

5.4   Summary and discussions

In order to find suitable conditions of the observation and the best choice of the polarization-phase curve parameter for estimating the surface properties of the target asteroid from the *in situ* and the limited polarimetric observation by MUSES-C, we investigated several kinds of relations between the parameters in the polarization-phase curve and the surface albedo, with emphasis on clarifying the effect of particle size on the surface, referring to previous observations and laboratory data and our laboratory measurements of layers consisting of olivine and graphite particles with different size distributions. It was found that the relationship between the slope of the polarization-phase curve and the albedo is dependent of particle size like the relationship between the maximum of polarization and the albedo. On the other hand, there is no dependence of particle size in the relationship between the minimum of polarization and the albedo. If

the minimum of polarization and the inversion angle will be determined, it may be possible to determine the asteroid type and distinguish whether the asteroid surface is covered by regolith layer or not.

For future works, we continue to investigate the possibility of estimation of asteroid surface properties by polarimetric observation by using various different samples, *i.e.* optical constants, size distribution of particles, porosity and so on.
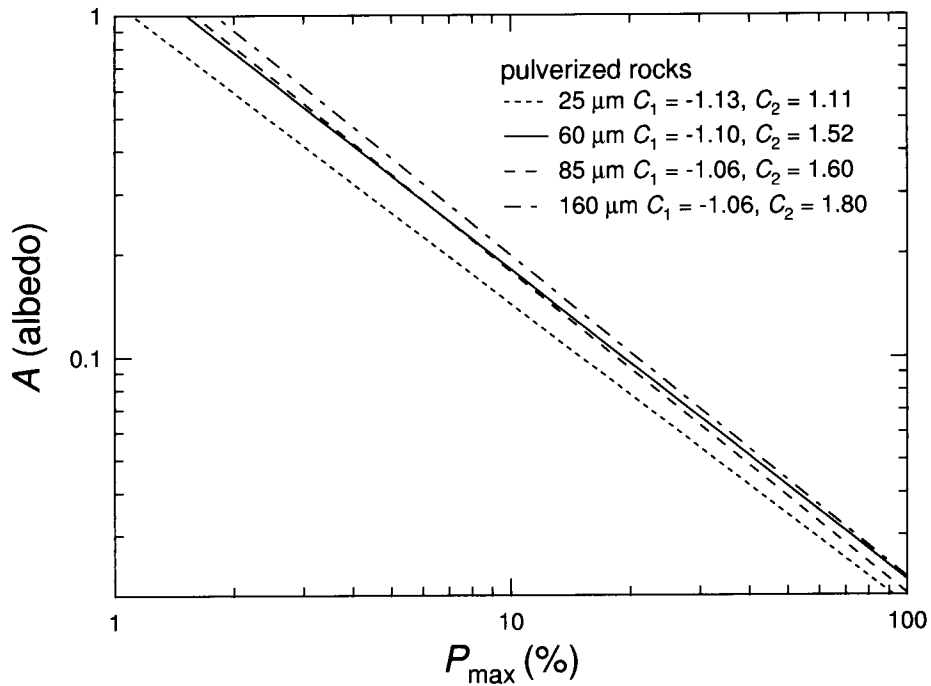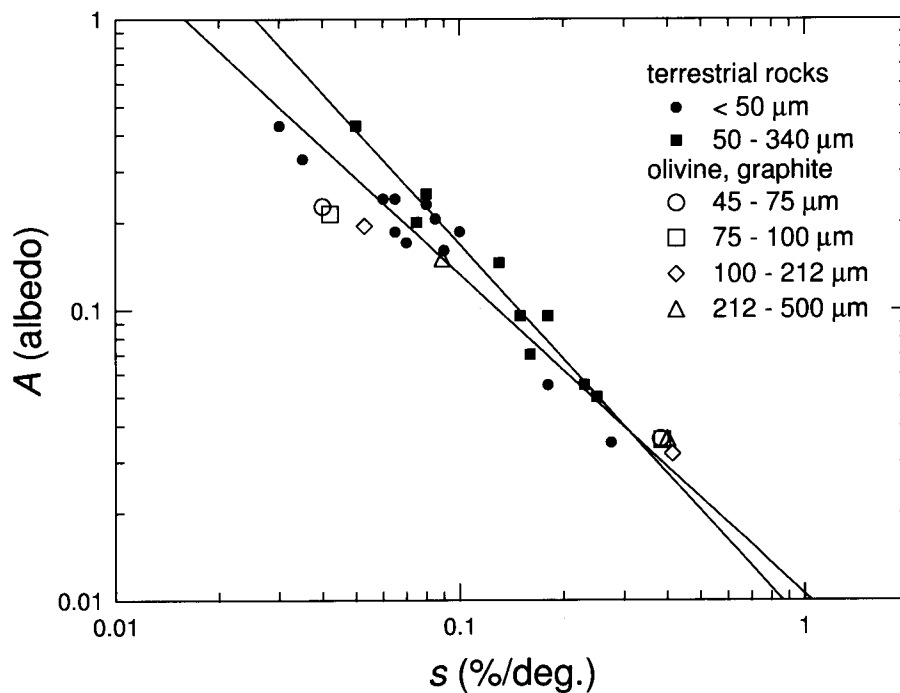
Fig. 5.2. Maximum of polarization P_{max} versus albedo A, for pulverized rocks sorted for four particle sizes (Dollfus 1999). Each particle size define a line represented by the equation: $\log P_{max} = C_1 \log A + \log C_2$.
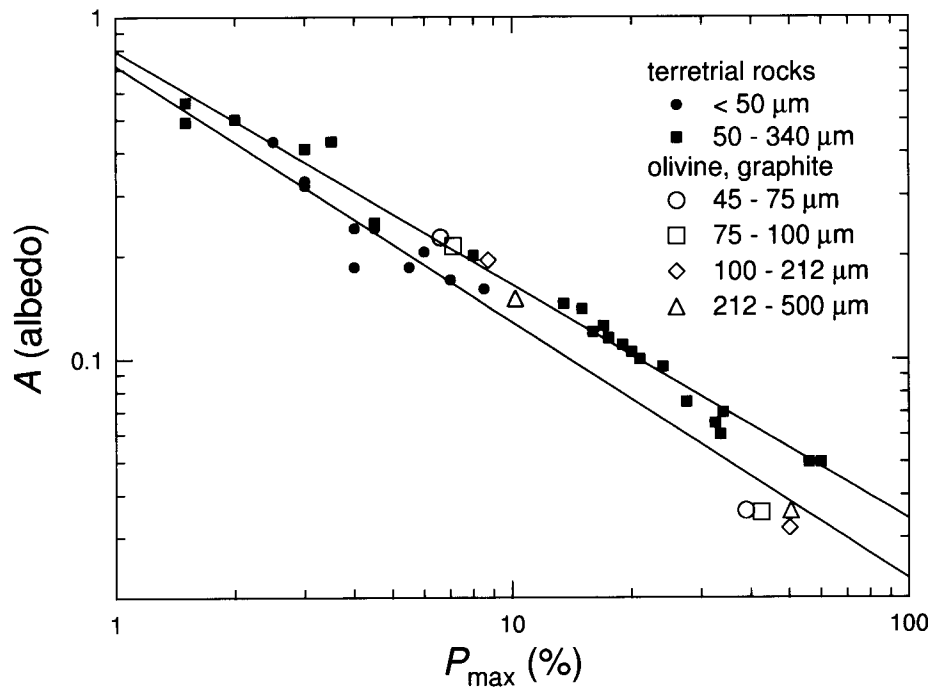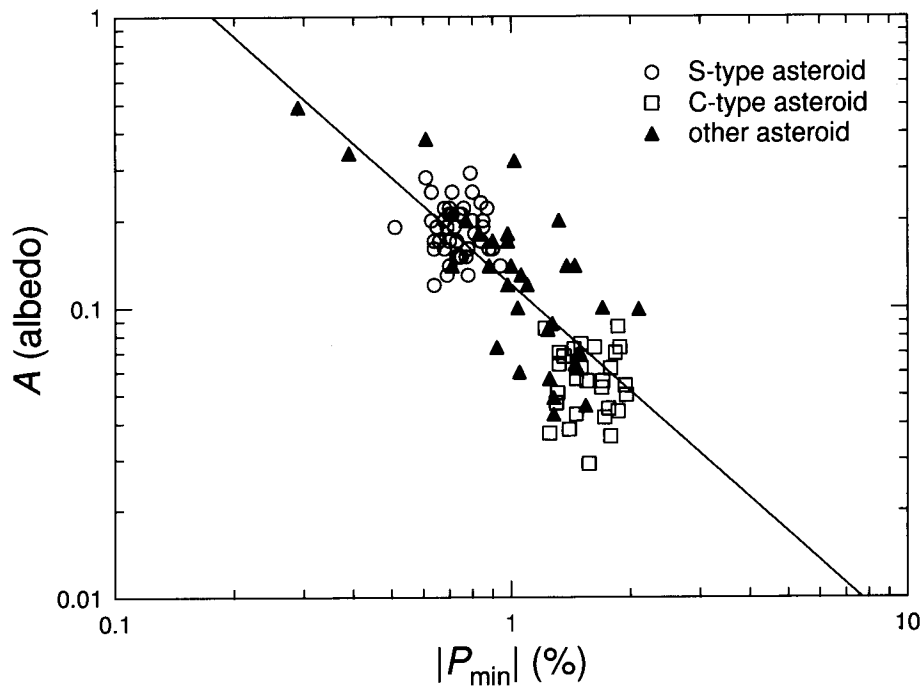

Fig. 5.3. Maximum of polarization P_{max} versus albedo A, for terrestrial rock (Geake and Dollfus 1986) and olivine and graphite particles (Kogachi 1999).

47
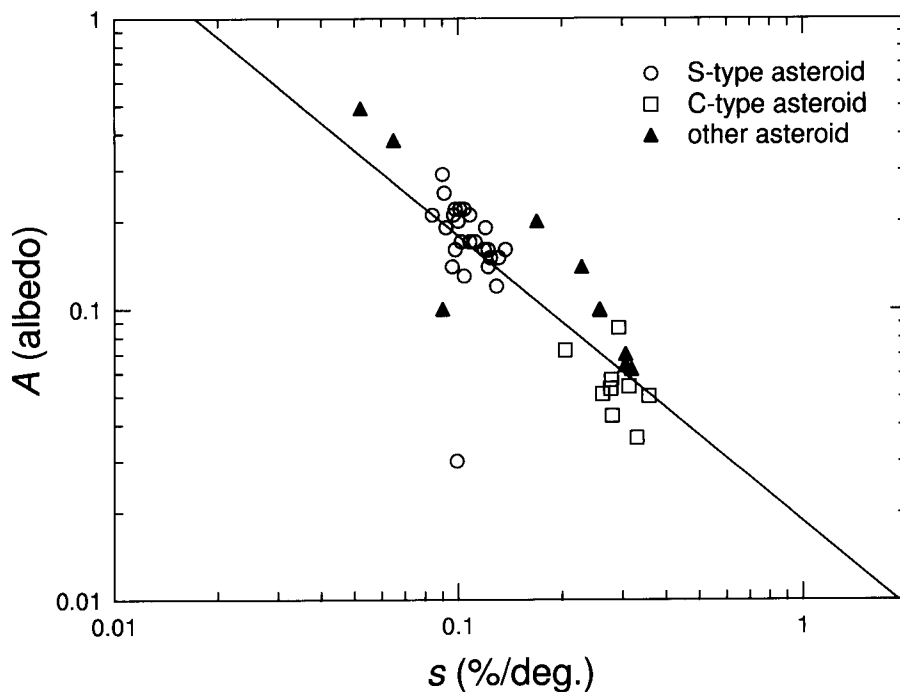
Fig. 5.4. Polarization curve slope s versus albedo A, for ground-based observations of asteroid. The straight line is empirical relationship by Lupishko and Mohamed (1996): $\log A = -0.98 \log s - 1.73$.

Fig. 5.5. Polarization curve slope s versus albedo A, for terrestrial rock (Geake and Dollfus 1986) and olivine and graphite particles (Kogachi 1999).

48

Fig. 5.6. Minimum of polarization P_{min} versus albedo A, for ground-based observations of asteroid. The straight line is empirical relationship by Lupishko and Mohamed (1996): $\log A = -1.22 \log P_{min} - 0.92$.
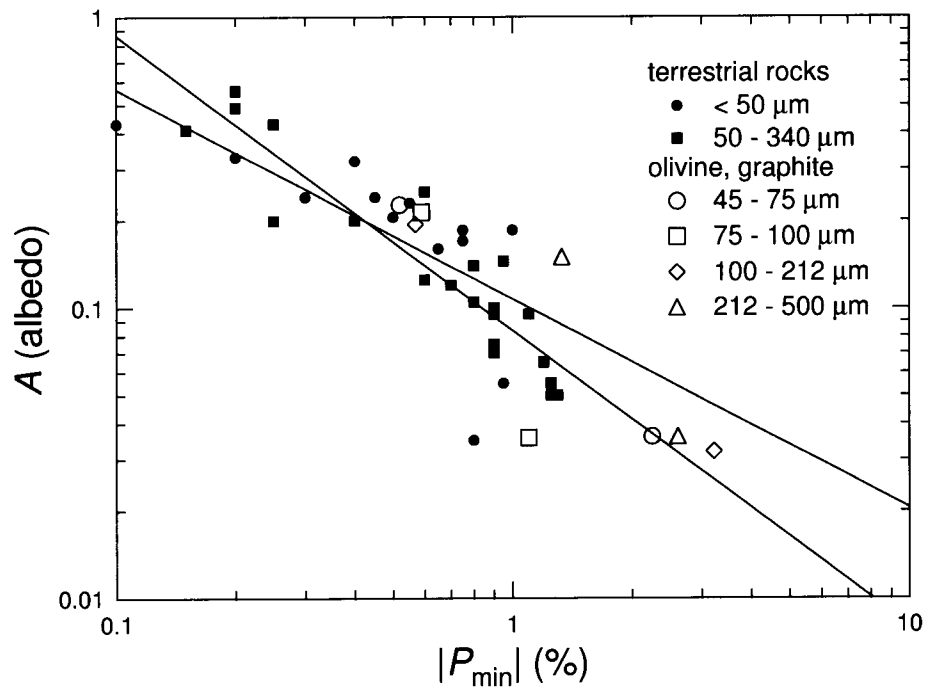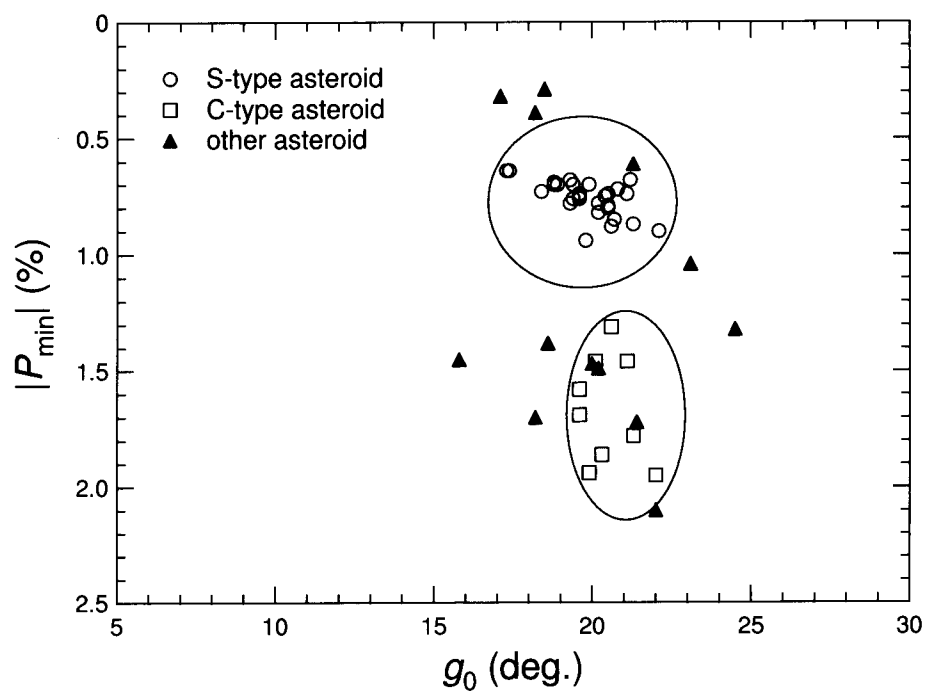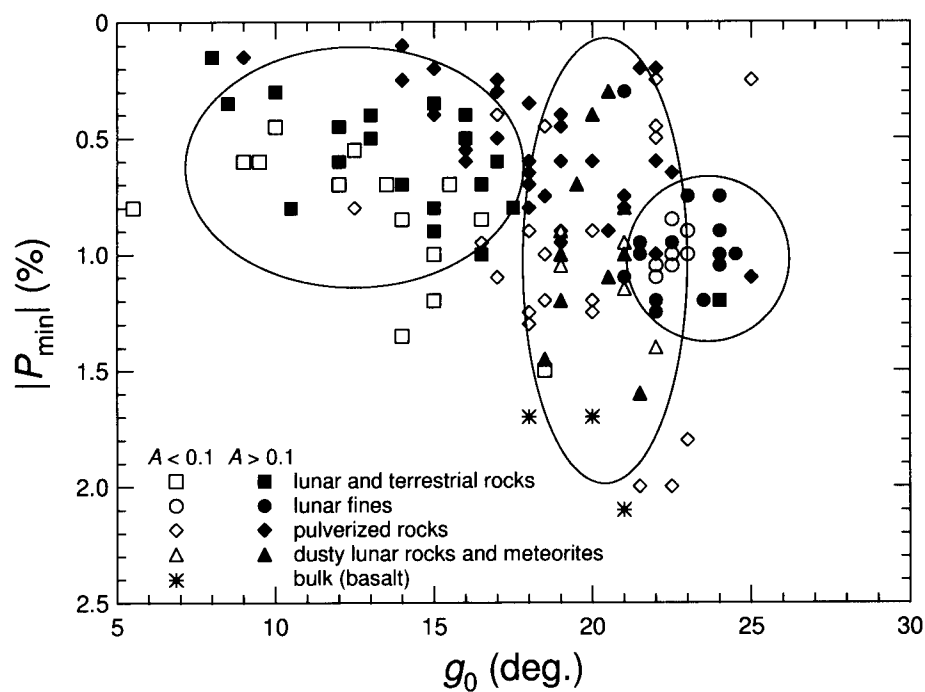

Fig. 5.7. Minimum of polarization P_{min} versus albedo A, for terrestrial rock (Geake and Dollfus 1986) and olivine and graphite particles (Kogachi 1999).

Fig. 5.8. Minimum of polarization P_{min} versus inversion angle g_0, for ground-based observations of asteroid.

Fig. 5.9. Minimum of polarization P_{min} versus inversion angle g_0, for lunar and terrestrial rocks, lunar fines, pulverized rocks and meteorites, dusty lunar rocks (Geake and Dollfus 1986), and bulks of basalt (Shepard and Arvidson 1999).

6 General Conclusions

Main purpose of this thesis is to investigate the light scattering by rough surfaces of small bodies in the solar system. Laboratory photo-polarimetric measurements of various types of rough surfaces, which are prepared as asteroid surface analogues, have been performed. Referring to the results of laboratory measurements of these samples, I summarized how the light scattering properties depend on the scattering geometry, roughness, particle size, and optical property of the surfaces. In addition, a comparison was made between laboratory data and Hapke's bidirectional reflectance model. These data will be useful in the analysis of the remote-sensing photo-polarimetric data in the future missions.

In section 2, the experimental instruments used for measurements in this thesis were explained in detail. The light source is a He-Ne laser at a wavelength of 632.8 nm and the detector is a photomultiplier. The incident and emergent angles to the surface are changed independently in a vertical plane. The minimum phase angle achieved for the central point of the sample is 1° for the moment. The sample surface can be also tilted from the horizontal position in parallel or perpendicular to the scattering plane. By adopting a chopping mode, it is possible to measure the optical signal and the dark level. The reflectance is calibrated using a standard white surface made of Ba_2SO_4. From the calibrations of the dark level, the stability, the sensitivity, and the linearity, this instruments is enable to measure the intensity and the state of the polarization of the scattered light.

In section 3, photometric measurements of scattered light by different types of rough surfaces were performed. The samples consist of alumina (Al_2O_3) plates, particles, and also combinations of both, i.e. two-component surface models of plates covered with thin layer of the particles, which are simulated the surface structure of small asteroids covered with a thin regolith layer. The average thickness was about 100 μm. The backscattered light reflectance by varying the incident angle to the surface at small phase angle (1°) and also the scattered light reflectance by varying the phase angle at normal incidence (0°) were measured. As expected, the existence of a thin layer of the particles on the smooth plates dilutes the Fresnel specular reflection by the plates. On the other hand, the opposition effect is added to the rough plate at small phase angles when it is covered with the thin layer of the particles. It is also expected from this work that if a regolith layer exists on an asteroid surface with a thickness much larger than 100 μm, the brightness of the asteroid surface at small phase angle might be relatively independent of incident angle.

In section 4, bidirectional reflectance of surfaces consisting of olivine, graphite, Allende meteorite, and Gao meteorite powders with different size distributions were measured in order to demonstrate how the retrieved Hapke parameters are changed depending on the range of phase angle. The measured coverage of phase angle were wide (2° − 155°), at 75° incident angle and narrow (2° − 80°), at 0° incident angle. All sample surfaces showed the forward scattering lobe in the large phase angle, as expected from the forward

single scattering character of natural soil particles. The sign of the retrieved asymmetry parameter for most samples derived from the data for wide range of phase angle using one-term Henyey-Greenstein phase function as a single-scattering particle phase function were positive. However, those for larger particles of Allende and Gao meteorite remain negative, but closer to zero than that for smaller particles. From this results it was confirmed that the one-term Henyey-Greenstein phase function, which is widely used in the previous works of bidirectional reflectance data, is not capable of describing the scattering behavior of particulate surfaces made of anisotropically scattering material which simultaneously displays significant forward and backward scattering components. The reason why the sign of the asymmetry parameter derived from the *in situ* observational data are negative value may be that the regolith particles of asteroids have meteorite like materials and larger sized particles.

In section 5, the empirical relations between the parameters in the polarization-phase curve and the surface albedo, including the dependence of the particle size distribution were investigated. The aim is to find the most suitable conditions of the observation and the best choice of polarization-phase curve parameter for estimating the surface properties of the target asteroid of MUSES-C, which plans limited polarimetric observations in the coverage of phase angle and the total number of the observations. From the laboratory results of the layers consisting of olivine and graphite particles with different size distributions, previous observation data, and other laboratory data, it was found that the relationship between the slope of the polarization-phase curve, which will be possible to determine from *in situ* measurements by MUSES-C, and the albedo is dependent of the size distribution of the regolith particles. Also it may be possible to determine the asteroid type and distinguish whether the asteroid surface is covered by regolith layer or not by using the plot of the minimum of polarization against the inversion angle.

Acknowledgement

References

[1] Bohren, C., and D. Huffmann 1983. *Absorption and Scattering of Light by Small Particles*. Wiley, New York.

[2] Bowell, E., A. Dollfus, B. Zellner, and J. E. Geake 1973. Polarimetric properties of the lunar surface and its interpretation Part 6: Albedo determination from polarimetric characteristics. *Proc. Lunar Sci. Conf. 4th*, pp. 3167-3174.

[3] Bowell, E., B. Hapke, D. Dominigue, K. Lumme, J. Peltoniemi, and A. W. Harris 1989. Application of photometric models to asteroids. In *Asteroids II* (R. Binzel, T. Gehrels, and M. S. Matthews, Eds.), pp. 524-556. Univ. of Arizona Press, Tucson.

[4] Chandrasekhar, S. 1960. *Radiative Transfer*. Dover, New York.

[5] Clark, B. E., J. Veverka, P. Helfenstein, P. C. Thomas, J. F. Bell III, A. Harch, M. S. Robinson, S. L. Murchie, L. A. McFadden, and C. R. Chapman 1999. NEAR photometry of asteroid 253 Mathilde. *Icarus* **140**, 53-65.

[6] Dollfus, A., M. Wolff, J. E. Geake, D. F. Lupishko, and L. M. Dougherty 1989. Photopolarimetry of asteroids. In *Asteroids II* (R. Binzel, T. Gehrels, and M. S. Matthews, Eds.), pp. 594-616. Univ. of Arizona Press, Tucson.

[7] Dollfus, A. 1998. Lunar surface imaging polarimetry: I. Roughness and grain size. *Icarus* **136**, 69-103.

[8] Drain, B., and J. Goodman 1993. Beyond Clausius-Masssotti: Wave propagation on a polarizable point lattice and the discrete dipole approximation. *Astrophys. J.* **405**, 685-697.

[9] Egan, W. G., J. Veverka, M. Noland, and T. Hilgeman 1973. Photometric and polarimetric properties of the Bruderheim chondritic meteorite. *Icarus* **19**, 358-371.

[10] French, L. M. 1980, *Photometric Properties of Carbonaceous Chondrites and Related Materials*. Ph. D. dissertation, Cornell Univ., Ithaca, NY.

[11] Fujiwara, A., T. Mukai, J. Kawaguchi, and K. T. Uesugi 1998. Sample return mission to NEA: MUSES-C. *Adv. Space Res.*, submitted.

[12] Geake, J. E., and A. Dollfus 1986. Planetary surface texture and albedo from parameter plots of optical polarization data. *Mon. Not. R. astr. Sor.* **218**, 75-91.

[13] Gervais, F. 1991. Aluminum Oxide. In *Handbook of Optical Constants of Solid II*, pp. 761-775. Academic Press.

[14] Hapke, B. 1993. *Theory of Reflectance and Emittance Spectroscopy*. Cambridge Univ. Press, Cambridge, UK.

[15] Hapke, B. 1996. Are planetary regolith particles back scattering? Response to a paper by M. Mishchenko. *J. Quant. Spectrosc. Radiat. Transfer* **55**, 837-848.

[16] Hapke, B., R. Nelson, and W. Smythe 1998. The opposition effect of the moon: Coherent backscatter and shadow hiding. *Icarus* **133**, 89-97.

[17] Helfenstein, P., and J. Veverka 1987. Photometric properties of lunar terrains derived from Hapke's equation. *Icarus* **72**, 342-357.

[18] Helfenstein, P., and J. Veverka, 1989. Physical characterization of asteroid surfaces from photometric analysis. In *Asteroids II* (R. Binzel, T. Gehrels, and M. S. Matthews, Eds.), pp. 557-593. Univ. of Arizona Press, Tucson.

[19] Helfenstein, P., J. Veverka, P. C. Thomas, D. P. Simonelli, P. Lee, K. Klaasen, T. V. Johnson, H. Breneman, J. Head, S. Murchie, F. Fanale, M. Robinson, B. E. Clark, J. Granahan, H. Garbeil, A. S. McEwen, R. Kirk, M. Davies, G. Neukum, S. Mottola, R. Wagner, M. Belton, C. Chapman, and C. Pilcher 1994. Galileo photometry of asteroid 951 Gaspra. *Icarus* **107**, 37-60.

[20] Helfenstein, P., J. Veverka, P. C. Thomas, D. P. Simonelli, K. Klaasen, T. V. Johnson, F. Fanale, J. Granahan, A. S. McEwen, M. Belton, and C. Chapman 1996. Galileo photometry of asteroid 243 Ida. *Icarus* **120**, 48-65.

[21] Hillier, J. K. 1997. Scattering of light by composite particles in a planetary surface. *Icarus* **130**, 328-335.

[22] Hudson, R. S., S. J. Ostro, and A. W. Harris 1997. Constraints on spin state and Hapke parameters of asteroid 4769 Castalia using lightcurves and a radar-derived shape model. *Icarus* **130**, 165-176.

[23] Hudson, R. S., and S. J. Ostro 1998. Photometric properties of asteroid 4179 Toutatis from lightcurves and a radar-derived physical model. *Icarus* **135**, 451-457.

[24] Iwasaki, S., and T. Mukai 1999. Simulation for light scattering by rough surface based on Kirchhoff's diffraction theory. *Adv. Space Res.* **23**, 1213-1216.

[25] Kogachi, M. 1999. Master thesis of the Graduate School of Science and Technology, Kobe University (in Japanese).

[26] Lupishko, D. F., and R. A. Mohamed 1999. A new calibration of the polarimetric albedo scale of asteroids. *Icarus* **119**, 209-213.

[27] McGuire, A. F., and B. W. Hapke 1995. An Experimental study of light scattering by large, irregular particles. *Icarus* **113**, 134-155.

[28] Mischenko, M. I. 1994. Asymmetry parameters of the phase function for densely packed scattering grains. *J. Quant. Spectrosc. Radiat. Transfer* **52**, 95-110.

[29] Mishchenko, M. I., and A. Macke 1997. Asymmetry parameters of the phase function for isolated and densely packed spherical particles with multiple internal inclusions in the geometric optics limit. *J. Quant. Spectrosc. Radiat. Transfer* **57**, 767-794.

[30] Nakamura, A. M., A. Kamei, M. Kogachi, and T. Mukai 1999. Laboratory measurements of laser-scattered light by rough surfaces. *Adv. Space Res.* **23**, 1201-1204.

[31] Oetking, P. 1966. Photometric studies of diffusely reflecting surfaces with application to the brightness of the moon. *J. Geophys. Res.* **71**, 2505-2513.

[32] Pollack, J., and J. Cuzzi 1980. Scattering by non-spherical particles of size comparable to a wavelength: A new semiempirical theory and its application to tropospheric aerosols. *J. Atmos. Sci.* **37**, 868-881.

[33] Purcell, E., and C. Pennypacker 1973. Scattering and absorption of light by non-spherical dielectric grains. *Astrophys. J.* **186**, 705-714.

[34] Shepard, K. M., and R. E. Arvidson 1999. The opposition surge and photopolarimetry of fresh and coated basalts. *Icarus* **141**, 172-178.

[35] Simonelli, D., M. Wisz, A. Switala, D. Adinolfi, J. Veverka, P. C. Thomas, and P. Helfenstein 1998. Photometric properties of Phobos surface materials from Viking images. *Icarus* **131**, 52-77.

[36] Statham, I. 1974. The relationship of porosity and angle of repose to mixture properties in assemblages of different sized materials. *Sedimentology* 21, 149-162.

[37] Thomas, P. C., D. Adinolfi, P. Helfenstein, D. Simonelli, and J. Veverka 1996. The surface of Deimos: Contribution of materials and processes to its unique appearance. *Icarus* **123**, 536-556.

[38] Van de Hulst, H. 1957. *Light Scattering by Small Particles*. Wiley, New York.

[39] Verbiscer, A. J., and J. Veverka 1990. Scattering properties of natural snow and frost: comparison with icy satellite photometry. *Icarus* **88**, 418-428.

[40] Zellner, B., M. Leake, T. Le Bertre, M. Duseaux, and A. Dollfus 1977. The asteroid albedo scale. I. Laboratory polarimetry of meteorites. *Proc. Lunar Sci. Conf.*, pp. 1091-1110.